Dyes and Pigments 217 (2023) 111388

Contents lists available at ScienceDirect

Dyes and Pigments

journal homepage: www.elsevier.com/locate/dyepig

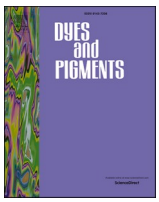

Intense millisecond-long red luminescence from heteroleptic Cu(I) 2,1,3-benzothiadiazole complexes

Valentina Ferraro [a,**], Matteo Girotto [a], Jesús Castro [b], Marco Bortoluzzi [a,c,*]

[a] Dipartimento di Scienze Molecolari e Nanosistemi, Università Ca' Foscari Venezia, Via Torino 155, 30170, Mestre, (VE), Italy
[b] Departamento de Química Inorgánica, Universidade de Vigo, Facultade de Química, Edificio de Ciencias Experimentais, 36310, (Galicia), Vigo, Spain
[c] Consorzio Interuniversitario Reattività Chimica e Catalisi (CIRCC), via Celso Ulpiani 27, 70126, Bari, Italy

ARTICLE INFO

Keywords:
Copper
2,1,3-Benzothiadiazole
Heteroleptic complexes
Luminescence
Millisecond lifetimes

ABSTRACT

Intense red-emitting heteroleptic Cu(I) complexes were isolated using 2,1,3-benzothiadiazole (BTD) as *N*-donor ligand and triphenylphosphine, bis[(2-diphenylphosphino)phenyl] ether (DPEphos) or bis(diphenylphosphino) methane (dppm) as *P*-donors. The structures of two mononuclear and one dinuclear derivatives with one nitrogen and two phosphorus atoms in the Cu(I) coordination sphere were ascertained by means of X-ray diffraction, revealing an overall tetrahedral geometry at the solid state due to the direct interaction of the counterion with Cu(I). Upon excitation with UV and violet-blue light, the Cu(I) complexes exhibited emissions centred between 623 and 683 nm with photoluminescence quantum yields up to 46%. Lifetimes in the tens-thousands millisecond range were observed. The values resulted affected by the choice of the counterion, and an increase of up to 15% was observed passing from tetrafluoroborate to perchlorate in the mononuclear BTD complex with two PPh_3 ligands. DFT calculations indicated that the lowest energy absorptions have charge transfer nature, from the $\{CuP_2\}$ fragments with the contributions of the *P*-bonded aryl substituents to an unoccupied π* orbital of BTD. The triplet→singlet emissions involve the metal centre, the phosphine ligands, and the occupied and empty orbitals of BTD.

1. Introduction

2,1,3-Benzothiadiazole (BTD) and its derivatives are nowadays successfully exploited for the preparation of luminescent materials to be applied for advanced technology as constituents of organic light-emitting diodes, solar cells, liquid crystals, photovoltaic cells and responsive dyes [1–11]. The π-extended heteroarene skeleton determines noteworthy withdrawing ability and well-ordered structures at the solid state thanks to chalcogen and π–π stacking interactions [12,13]. *N*-donor ligands based on the BTD moiety were widely used for the synthesis of luminescent coordination compounds and metal-organic frameworks of d- and f-block elements, efficiently applied in selected cases as molecular probes [14–21].

New avenues for the preparation of more sustainable light-emitting devices consider copper- and carbon-based materials as key building blocks [22]. Cu(I) is one of the most investigated first-row transition metal centres for the replacement of expensive, rare and geopolitically problematic elements in lighting technology [23–31], besides being of interest for sustainable photoactivated reactions and photocatalysis [32–35]. The photophysical properties of Cu(I) complexes, often related to the population of MLCT excited states, are adjustable, including the colour of the emission. The closed-shell d^{10} ground state configuration circumvents the problem of non-radiative deactivation of excited states via low-lying metal-centred states. Moreover, Cu(I) complexes can exhibit peculiar features ascribable to thermally activated delayed fluorescence (TADF), appealing for electroluminescent devices thanks to the possibility of harvesting both singlet and triplet excitons [36–43].

The combination of Cu(I) and the BTD heterocycle represents a potentially intriguing approach to obtain sustainable complexes with enhanced luminescent properties. In recent years, several azoles proved to be promising building blocks for the synthesis of suitable ligands in the field of Cu(I) luminescent compounds [44–67]. For instance, bidentate [N,N']-ligands constituted by a benzooxazole heterocycle functionalized with a six-membered aromatic *N*-donor afforded highly luminescent heteroleptic Cu(I) complexes, whose absorptions and emissions were influenced by the angle between the ancillary *P*-donor

* Corresponding author. Dipartimento di Scienze Molecolari e Nanosistemi, Università Ca' Foscari Venezia, Via Torino 155, 30170, Mestre, (VE), Italy.
** Corresponding author.
E-mail addresses: valentina.ferraro@unive.it (V. Ferraro), markos@unive.it (M. Bortoluzzi).

https://doi.org/10.1016/j.dyepig.2023.111388
Received 11 April 2023; Received in revised form 2 May 2023; Accepted 8 May 2023
Available online 10 May 2023

moieties and by the interconversion among polymorphic structures [68–71]. The presence of a sulphur atom in the *N*-donor structure could enhance the photophysical properties of the corresponding Cu(I) complexes, as observed for instance by Housecroft, Constable and co-workers in heteroleptic di(methylsulfanyl)-1,10-phenanthroline Cu (I) complexes [72]. The investigations reported in the literature on Cu(I) BTD derivatives are however limited to coordination polymers, such as those formed by reacting BTD with CuCl [73], $[Cu(NCCH_3)_4][PF_6]$ and Cu/CuX_2 ($X^- = NO_3^-$, ClO_4^-) [74], whose emissive features were not investigated. The coordination polymer isolated in 2022 by reacting CuI and BTD showed an emission band centred in the NIR range, with temperature-dependent lifetime [75]. Considering selected BTD derivatives, dinuclear complexes were isolated by reacting Cu(I) precursors with 4-amino-2,1,3-benzothiadiazole, but also in this case the luminescence was not studied [76]. Recently, the ligands *N*,*N*-bis (diphenylphosphanyl)-2,1,3-benzothiadiazol-4-amine and N,N′-bis(2,1, 3-benzothiadiazol-4-yl)-1-phenylphosphanediamine were prepared starting from 4-amino-2,1,3-benzothiadiazole. The Cu(I) coordination polymer obtained from the first ligand, containing Cu–N(BTD) and Cu–P bonds, showed temperature-dependent emission in the red range [77, 78].

Our research group is currently interested in the preparation of luminescent BTD derivatives, and we recently reported the synthesis and luminescent solvatochromic properties of *N*,*N*-dimethyl-4-amino-2,1,3-benzothiadiazole [79]. In this paper we describe the synthesis and photoluminescence of cationic heteroleptic Cu(I) complexes with BTD as *N*-donor. The compounds showed intense emissions in the red region of the visible spectrum, with lifetimes in the milliseconds range dependent upon the choice of the phosphine and of the counterion.

2. Experimental section

2.1. Materials and methods

Commercial solvents (Merck) were purified following reported procedures to be used inside the glove-box [80]. All the other reagents were Sigma Aldrich products used as received. Cu(I) precursors were prepared following reported methods [81–84]. The syntheses of the complexes starting from $[Cu(NCCH_3)_4][BF_4]$ and CuCl were carried out under inert atmosphere in a glove-box (MBraun Labstar with MB 10 G gas purifier) filled with N_2 and equipped for inorganic syntheses. The reactions starting from $[Cu(\kappa^2\text{-}BH_4)(PPh_3)_2]$ were conducted using standard Schlenk techniques.

Elemental analyses (C, H, N, S) were carried out using an Elementar Unicube microanalyzer. Conductivity measurements in acetone were performed with a Radiometer Copenhagen CDM83 instrument. Melting point measurements were carried out using a modified Falc 360 D apparatus equipped with a video recording device. IR spectra (KBr pellets) were collected in the range of 4000–400 cm^{-1} using a PerkinElmer Spectrum One spectrophotometer. Heteronuclear magnetic resonance (NMR) spectra were collected at variable temperatures employing Bruker Avance 300 and Avance 400 instruments operating respectively at 300.13 MHz and 400.13 MHz of ^1H resonance. ^1H and $^{13}C\{^1H\}$ NMR spectra are referred to the partially non-deuterated fraction of the solvent, itself quoted to tetramethylsilane. $^{31}P\{^1H\}$ NMR spectra are referred to 85% H_3PO_4 in water. Cyclic voltammetry measurements were performed using an eDAQ ET014-199 instrument in acetone containing 0.1 M $LiClO_4$. All the measurements were carried out under argon at room temperature. The working electrode was 1-mm glassy carbon disk eDAQ ET074-1, while the auxiliary electrode was Pt-coated titanium rod eDAQ ET078-1. Ferrocene was introduced as internal standard and a Pt wire was used as pseudo-reference electrode.

CAUTION: perchlorate salts of transition metal complexes are potentially explosive and should be handled with care.

2.2. Synthesis and characterization of the complexes

2.2.1. Synthesis and characterization of $\mathbf{1^{BF4}}$ and $\mathbf{2^{BF4}}$

0.3 mmol of $[Cu(\kappa^2\text{-}BH_4)(PPh_3)_2]$ (0.181 g) or $[Cu(\kappa^2\text{-}BH_4)$(DPEphos] (0.185 g) and 0.3 mmol of BTD (0.041 g) were dissolved in 50 mL of dichloromethane. The solution was cooled at 77 K with a nitrogen bath and put under inert atmosphere. 41 μL of $HBF_4{\cdot}Et_2O$ (0.3 mmol) were added through a syringe and the reaction mixture was allowed to slowly warm up to room temperature. After stirring overnight, the solution was purified by filtration and dichloromethane was evaporated under reduced pressure. The addition of diethyl ether (20 mL) caused the separation of a solid, that was filtered, washed with 5 mL of diethyl ether and dried under vacuum. Yield: 63% (0.153 g) for $\mathbf{1^{BF4}}$, 67% (0.166 g) for $\mathbf{2^{BF4}}$. Crystals of $\mathbf{1^{BF4}}$ suitable for X-ray diffraction were collected from the evaporation of diethyl ether solutions.

$\mathbf{1^{BF4}}$. Anal. calcd for $C_{42}H_{34}BCuF_4N_2P_2S$ (811.1 g mol^{-1}, %): C, 62.19; H, 4.23; N, 3.45; S, 3.95. Found (%): C, 61.94; H, 4.25; N, 3.44; S, 3.93. M. p. 155 °C (dec.). Λ_M (acetone, 298 K): 149 $\Omega^{-1}mol^{-1}cm^2$. ^1H NMR ($CDCl_3$, 213 K) δ 8.01 (m, 2H, BTD), 7.65 (m, 2H, BTD), 7.40 (t, $^3J_{HH}$ = 7.5 Hz, 6H, Ph), 7.15 (t, $^3J_{HH}$ = 7.4 Hz, 12H, Ph), 6.90 (m, 12H, Ph). $^{31}P\{^1H\}$ NMR ($CDCl_3$, 298 K) δ 0.4 (FWHM = 85 Hz). $^{13}C\{^1H\}$ NMR ($CDCl_3$, 298 K) δ 154.7 (C_{ipso}, BTD), 133.6 (PPh_3), 130.7 (PPh_3), 129.5 (BTD), 129.1 (PPh_3), 121.5 (BTD). *P*-bonded carbons not assigned. IR (KBr, cm^{-1}): 3100-3020 m/w (aromatic $\nu_{C\text{-}H}$), 2980-2850 m/w (ν_{CH}); 1480-1385 m/w (aromatic ν_{CC} and ν_{CN}); 1085 s (ν_{BF4}). UV-VIS (CH_2Cl_2, 298 K, nm): <360, 311, 305, 299, 257 (sh).

$\mathbf{2^{BF4}}$. Anal. calcd for $C_{42}H_{32}BCuF_4N_2OP_2S$ (825.08 g mol^{-1}, %): C, 61.14; H, 3.91; N, 3.40; S, 3.89. Found (%): C, 60.90; H, 3.93; N, 3.41; S, 3.74. M. p. > 230 °C (dec.). Λ_M (acetone, 298 K): 150 $\Omega^{-1}mol^{-1}cm^2$. ^1H NMR ($CDCl_3$, 298 K) δ 8.03 (m, 2H, BTD), 7.62 (m, 2H, BTD), 7.37–7.16 (m, 20H, DPEphos), 6.98 (t, $^3J_{HH}$ = 7.4 Hz, 2H, DPEphos), 6.84–6.65 (m, br, 6H, DPEphos). $^{31}P\{^1H\}$ NMR ($CDCl_3$, 298 K) δ −17.6 (FWHM = 105 Hz). IR (KBr, cm^{-1}): 3070-3010 m/w (aromatic ν_{CH}), 2980-2920 m/w (ν_{CH}); 1480-1440 m/w (aromatic ν_{CC} and ν_{CN}); 1085 s (ν_{BF4}). UV-VIS (CH_2Cl_2, 298 K, nm): <360, 290.

2.2.2. Synthesis of $\mathbf{1^{An}}$ and **3**

0.472 g of $[Cu(NCCH_3)_4][BF_4]$ (1.5 mmol) were dissolved in 20 mL of dry dichloromethane inside the glove box. 3.0 mmol of triphenylphosphine (0.787 g) or 1.5 mmol of bis(diphenylphosphino)methane (dppm) (0.577 g) were added to the solution. After stirring for 4 h, 0.205 g of 2,1,3-benzothiadiazole (1.5 mmol) were added and the solution was stirred overnight. The solvent was then evaporated under reduced pressure and, after adding diethyl ether, the solid was filtered, washed and dried under vacuum. Yield: 65% (0.831 g) for $\mathbf{1^{An}}$, 60% (0.561 g) for **3**. Crystals of **3** suitable for X-ray diffraction were collected from dichloromethane/diethyl ether solutions.

$\mathbf{1^{An}}$. Anal. calcd for $C_{44}H_{37}BCuF_4N_3P_2S$ (852.15 g mol^{-1}, %): C, 62.02; H, 4.38; N, 4.93; S, 3.76. Found (%): C, 61.77; H, 4.40; N, 4.91; S, 3.74. M.p. 130 °C (dec.). Λ_M (acetone, 298 K): 193 $\Omega^{-1}mol^{-1}cm^2$. ^1H NMR ($CDCl_3$, 298 K) δ 7.99 (m, 2H, BTD), 7.62 (m, 2H, BTD), 7.47 (m, 6H, Ph), 7.42–7.24 (m, 24H, Ph), 2.29 (s, 3H, CH_3CN). ^1H NMR ($CDCl_3$, 213 K) δ 7.90 (m, 2H, BTD), 7.65 (m, 2H, BTD), 7.41 (m, 6H, Ph), 7.27 (m, 12H, Ph), 7.11 (m, 12H, Ph), 2.32 (s, 3H, CH_3CN). $^{31}P\{^1H\}$ NMR ($CDCl_3$, 213 K) δ −0.9 (FWHM = 35 Hz). $^{13}C\{^1H\}$ NMR ($CDCl_3$, 298 K) δ 154.4 (C_{ipso}, BTD), 133.6 (d, J_{PC} = 12.4 Hz, PPh_3), 130.8 (PPh_3), 129.9 (BTD), 129.1 (PPh_3), 121.4 (BTD), 2.5 ($NCCH_3$). *P*-bonded and C≡N carbons not assigned. IR (KBr, cm^{-1}): 3070-3000 m/w (aromatic ν_{CH}), 1480-1440 m/s (aromatic ν_{CC} and ν_{CN}), 1120-1000 m (ν_{BF4}). UV-VIS (CH_2Cl_2, 298 K, nm): <360, 312, 305, 300, 255 (sh).

3. Anal. calcd for $C_{58}H_{51}B_2Cu_2F_8N_3P_4S$ (1246.71 g mol^{-1}, %): C, 55.88; H, 4.12; N, 3.37; S, 2.57. Found (%): C, 55.66; H, 4.14; N, 3.36; S, 2.56. M.p. 145 °C (dec.). Λ_M (acetone, 298 K): 257 $\Omega^{-1}mol^{-1}cm^2$. ^1H NMR ($CDCl_3$, 298 K) δ 7.83 (m, 2H, BTD), 7.54 (m, br, 2H, BTD), 7.40–7.15 (m, 40H, dppm), 3.74 (m, br, 4H, dppm), 2.31 (s, 3H, CH_3CN). $^{31}P\{^1H\}$ NMR ($CDCl_3$, 298 K) δ −12.3 (FWHM = 20 Hz). ^{13}C

{^{1}H} NMR ($CDCl_3$, 298 K) δ 154.1 (C_{ipso}, BTD), 132.7 (dppm), 131.0 (dppm), 130.0 (BTD), 129.22 (dppm), 121.2 (BTD), 25.4 (dppm), 2.6 ($NCCH_3$). C_{ipso} not assigned. IR (KBr, cm^{-1}): 3100-3000 m/w (aromatic ν_{CH}), 2990-2850 m/w (ν_{CH}), 2280 w ($\nu_{C\equiv N}$), 1480-1440 m/s (aromatic ν_{CC} and ν_{CN}), 1100-995 m (ν_{BF4}). UV-VIS (CH_2Cl_2, 298 K, nm): <360, 312, 306.

2.2.3. Synthesis of $\mathbf{1}^{ClO4}$, $\mathbf{2}^{ClO4}$ and **4**

0.100 g of CuCl (1.0 mmol) were suspended in 15 mL of dry dichloromethane and 2.0 mmol of triphenylphosphine (0.525 g), or 1.0 mmol of DPEphos (0.539 g) or dppm (0.384 g) were added. After the complete dissolution of CuCl, a stoichiometric amount of benzothiadiazole (1.0 mmol, 0.136 g) was added and the solution suddenly became yellow coloured. Then 0.207 g of $AgClO_4$ (1.0 mmol) were added and the mixture was left overnight under stirring. The AgCl formed was separated by centrifugation. The solvent was evaporated under reduced pressure to afford an oil that was triturated with diethyl ether. The so-obtained solid was filtered, washed with diethyl ether and dried under vacuum. Yield: 71% (0.585 g) for $\mathbf{1}^{ClO4}$, 75% (0.628 g) for $\mathbf{2}^{ClO4}$, 73% (0.500 g) for **4**. Crystals of $\mathbf{1}^{ClO4}$ suitable for X-ray diffraction were collected from dichloromethane/diethyl ether solutions.

$\mathbf{1}^{ClO4}$. Anal. calcd for $C_{42}H_{34}ClCuN_2O_4P_2S$ (823.74 g mol^{-1}, %): C, 61.24; H, 4.16; N, 3.40; S, 3.89; Cl, 4.30. Found (%): C, 61.22; H, 4.18; N, 3.27; S, 3.74; Cl, 4.32. M.p. 162 °C (dec.). Λ_M (acetone, 298 K): 149 $\Omega^{-1}mol^{-1}cm^2$. ^{1}H NMR ($CDCl_3$, 298 K) δ 7.91 (m, 2H, BTD), 7.55 (m, 2H, BTD), 7.47–7.21 (m, br, 30H, PPh_3). ^{31}P{^{1}H} NMR ($CDCl_3$, 298 K) δ −0.1 (FWHM = 180 Hz). ^{13}C{^{1}H} NMR ($CDCl_3$, 298 K) δ 154.5 (C_{ipso}, BTD), 133.8 (d, J_{PC} = 12.0 Hz, PPh_3), 130.6 (PPh_3), 129.7 (BTD), 129.0 (PPh_3), 121.5 (BTD). *P*-bonded carbons not assigned. IR (KBr, cm^{-1}): 3090-2990 m/w (aromatic ν_{CH}), 1535-1440 m/s (aromatic ν_{CC} and ν_{CN}), 1120 s (ν_{ClO4}). UV-VIS (CH_2Cl_2, 298 K, nm): <350, 312, 305, 298, 248 (sh).

$\mathbf{2}^{ClO4}$. Anal. calcd for $C_{42}H_{32}ClCuN_2O_5P_2S$ (837.73 g mol^{-1}, %): C, 60.22; H, 3.85; N, 3.34; S, 3.83; Cl, 4.23. Found (%): C, 60.15; H, 3.87; N, 3.35; S, 3.81; Cl, 4.21. M.p. 200 °C (dec.). Λ_M (acetone, 298 K): 90 $\Omega^{-1}mol^{-1}cm^2$. ^{1}H NMR ($CDCl_3$, 298 K) δ 7.97 (m, 2H, BTD), 7.56 (m, 2H, BTD), 7.37–7.26 (m, br, 12H, DPEphos), 7.21 (m, br, 8H, DPEphos), 6.98 (t, 2H, $^3J_{HH}$ = 7.6 Hz, DPEphos), 6.81–6.53 (m, br, 6H, DPEphos). ^{31}P{^{1}H} NMR ($CDCl_3$, 298 K) δ −16.1 (FWHM = 192 Hz). ^{13}C{^{1}H} NMR ($CDCl_3$, 298 K) δ 157.7 (C_{ipso}, DPEphos), 154.5 ($C_{ipso,}$ BTD), 134.0 (DPEphos), 133.9 (t, J_{PC} = 7.7 Hz, DPEphos), 132.0 (DPEphos), 130.6 (DPEphos), 129.6 (BTD), 129.0 (t, J_{PC} = 4.9 Hz, DPEphos), 124.8 (DPEphos), 121.4 (BTD), 119.5 (DPEphos). *P*-bonded carbons not assigned. IR (KBr, cm^{-1}): 3080-2990 m/w (aromatic ν_{CH}), 1525-1385 m/s (aromatic ν_{CC} and ν_{CN}), 1140-1050 s (ν_{ClO4}). UV-VIS (CH_2Cl_2, 298 K, nm): <360, 270.

4. Anal. calcd for $C_{62}H_{52}Cl_2Cu_2N_4O_8P_4S_2$ (1367.12 g mol^{-1}, %): C, 54.47; H, 3.83; N, 4.10; S, 4.69; Cl, 5.19. Found (%): C, 54.26; H, 3.85; N, 4.08; S, 4.67; Cl, 5.21. M.p. 200 °C (dec.). Λ_M (acetone, 298 K): 196 $\Omega^{-1}mol^{-1}cm^2$. ^{1}H NMR ($CDCl_3$, 298 K) δ 7.98 (m, br, 4H, BTD), 7.59 (m, br, 4H, BTD), 7.22–7.08 (m, 24H, dppm), 7.01 (t, 16H, $^3J_{HH}$ = 7.6 Hz, dppm), 3.40 (m, br, 4H, dppm). ^{31}P{^{1}H} NMR ($CDCl_3$, 298 K) δ −13.0 (FWHM = 30 Hz). ^{13}C{^{1}H} NMR ($CDCl_3$, 298 K) δ 133.4 (BTD), 132.6 (dppm), 130.4 (dppm), 129.7 (BTD), 128.8 (dppm), 121.5 (BTD), 26.7 (dppm). C_{ipso} not assigned. IR (KBr, cm^{-1}): 3090-2990 m/w (aromatic ν_{CH}), 2950–2900 (ν_{CH}), 1530-1440 m/s (aromatic ν_{CC} and ν_{CN}), 1160-1030 s (ν_{ClO4}). UV-VIS (CH_2Cl_2, 298 K, nm): <340, 250, 267 (sh), 275 (sh), 285 (sh), 296 (sh), 302 (sh), 309 (sh).

2.3. Crystal structure determination

Crystallographic data were collected at CACTI (Univ. of Vigo) at 100 K (CryoStream 800) using a Bruker D8 Venture Photon II CMOS detector and Mo-Kα radiation (λ = 0.71073 Å) generated by an Incoatec Microfocus Source IμS. The software APEX3 was used for collecting frames of data, indexing reflections, and the determination of lattice parameters, SAINT for integration of intensity of reflections, and SADABS for scaling and empirical absorption correction [85]. The crystallographic treatment was performed with the Oscail program [86], solved using the SHELXT program [87]. The structure was subsequently refined by a full-matrix least-squares based on F^2 using the SHELXL program [88]. Non-hydrogen atoms were refined with anisotropic displacement parameters. Hydrogen atoms were included in idealized positions and refined with isotropic displacement parameters. For $\mathbf{1}^{ClO4}$, the coordinated perchlorate anion resulted to be disordered, and two of the oxygen atoms were modelled over two positions with occupancy factors 0.585 (14):0.415(14). In the case of the dimeric compound **3** a non-merohedral twinning was found in the last stages of the refinement (β angle is about 92.6°) and was treated by using TWINROTMATR subroutine in PLATON. After this treatment, some atoms are disordered, but they were not modelled further. CCDC 2242770–2242772 contain the supplementary crystallographic data for this paper. These data can be obtained free of charge from the Cambridge Crystallographic Data Centre via www.ccdc.cam.ac.uk/data_request/cif. PLATON (version 60720) was used to obtain some geometrical parameters from the cif files [89].

2.4. Photoluminescence measurements

Absorption spectra in dichloromethane solutions were collected using a PerkinElmer Lambda 40 spectrophotometer. Photoluminescence measurements on solid samples were carried out using air-tight quartz sample holders, filled in glove-box to avoid interactions of the complexes with moisture. Photoluminescence emission (PL) and excitation (PLE) measurements were carried out at room temperature on solid samples with Horiba Jobin Yvon Fluorolog-3 spectrofluorometer. A continuous-wave xenon arc lamp was used as source selecting the excitation wavelength by a double Czerny–Turner monochromator. A single grating monochromator coupled to a photomultiplier tube was used as detection system for optical emission measurements. Excitation and emission spectra were corrected for the instrumental functions. Time-resolved analyses were performed in multi-channel scaling modality (MCS) by using a pulsed UV led sources (Horiba SpectraLEDs) centred at 290 or 445 nm. Photoluminescence quantum yield Φ of the complexes (solid state, r.t.) was measured using an OceanOptics HR4000CG UV-NIR detector, fiber-coupled to an integrating sphere connected to an OceanOptics LED source centred at 365 nm. The values were reported as the average of three measurements. The same spectrometer, coupled with an OceanOptics fibre QR400-7-SR-BX and an OceanOptics DH-2000-BAL deuterium-halogen lamp was used to record reflectance spectra at room temperature.

2.5. Computational details

Geometry optimizations were carried out using the global-hybrid *meta*-NGA functional MN15 DFT functional and the Ahlrichs and Weigend's def2 split-valence polarized basis set [90,91]. The *C*-PCM implicit solvation model was added to MN15 calculations, considering dichloromethane as continuous medium [92,93]. The relative energies of the excited states were obtained by carrying out TD-DFT (time--dependent DFT) calculations at the same theoretical level, starting from singlet and triplet state geometries [94]. Calculations were carried out using Gaussian 16 [95] and the output files were analysed with Multiwfn, version 3.8 [96,97]. Cartesian coordinates of the DFT-optimized structures are provided in the Supplementary file. The percent buried volume ($V\%_{bur}$) was calculated with the SAMBVCA 2.1 program [98], using the default parameters (bond radii scaled by 1.17, sphere radius 3.5 Å). All the atoms were considered, and the centre of the sphere was put on the Cu atom. The Cartesian coordinates used were obtained from the.cif files.

3. Results and discussion

3.1. Synthesis, characterization and X-ray structure determination of the complexes

The investigation on heteroleptic Cu(I) complexes with BTD in the coordination sphere began using Cu(I)-borohydride precursors, following the conditions previously described by our research group [81]. The decomposition of the borohydride ligand with $HBF_4{\cdot}Et_2O$ followed by the addition of BTD afforded the heteroleptic complexes $\mathbf{1}^{\mathbf{BF4}}$ and $\mathbf{2}^{\mathbf{BF4}}$ (see Scheme 1). The formulation of the products did not change also working with an excess of BTD. A different synthetic approach, based on the stepwise substitution of the ligands in $[Cu(NCCH_3)_4][BF_4]$ with PPh_3 and BTD, afforded the complex $\mathbf{1}^{\mathbf{An}}$, where the retention of an acetonitrile molecule in the coordination sphere is proposed on the basis of experimental data. The use of the bidentate phosphine dppm instead of PPh_3 allowed the isolation of the unsymmetrical dinuclear complex **3** depicted in Scheme 1, where one Cu(I) interacts with a BTD ligand, while the other one with an acetonitrile molecule. Quite surprisingly, the complete displacement of acetonitrile from Cu(I) was not achieved also carrying out the reactions overnight with an excess of BTD. Cu(I) BTD derivatives without coordinated acetonitrile were obtained employing CuCl as precursor. The addition of the chosen phosphine to a suspension of CuCl in dichloromethane determined its solubilisation. BTD was then added in the presence of Ag(I) perchlorate and, after work-up, the complexes $\mathbf{1}^{\mathbf{ClO4}}$, $\mathbf{2}^{\mathbf{ClO4}}$ and **4** were isolated.

As described below, $\mathbf{1}^{\mathbf{BF4}}$, $\mathbf{1}^{\mathbf{ClO4}}$ and **3** were structurally characterized. According to experimental and DFT outcomes, the formula $[Cu(NCCH_3)(BTD)(PPh_3)_2][BF_4]$ is proposed for $\mathbf{1}^{\mathbf{An}}$. The possible geometries of $\mathbf{2}^{\mathbf{BF4}}$ and $\mathbf{2}^{\mathbf{ClO4}}$ are more ambiguous, and DFT calculations suggested the formation of polynuclear compounds with bridging BTD. Finally, thanks to the similarity with compound **3** and according to DFT outcomes, a dinuclear structure for **4** with bridging dppm ligands is proposed in Scheme 1.

The proposed formulae were supported by elemental analysis data and conductivity measurements in acetone, where the complexes behaved as 1:1 or 1:2 electrolytes. The IR spectra showed aromatic ν_{CH}, ν_{CC} and ν_{CN} stretchings associated with the coordinated phosphines and BTD, besides the stretchings of the BF_4^- and ClO_4^- counterions in the

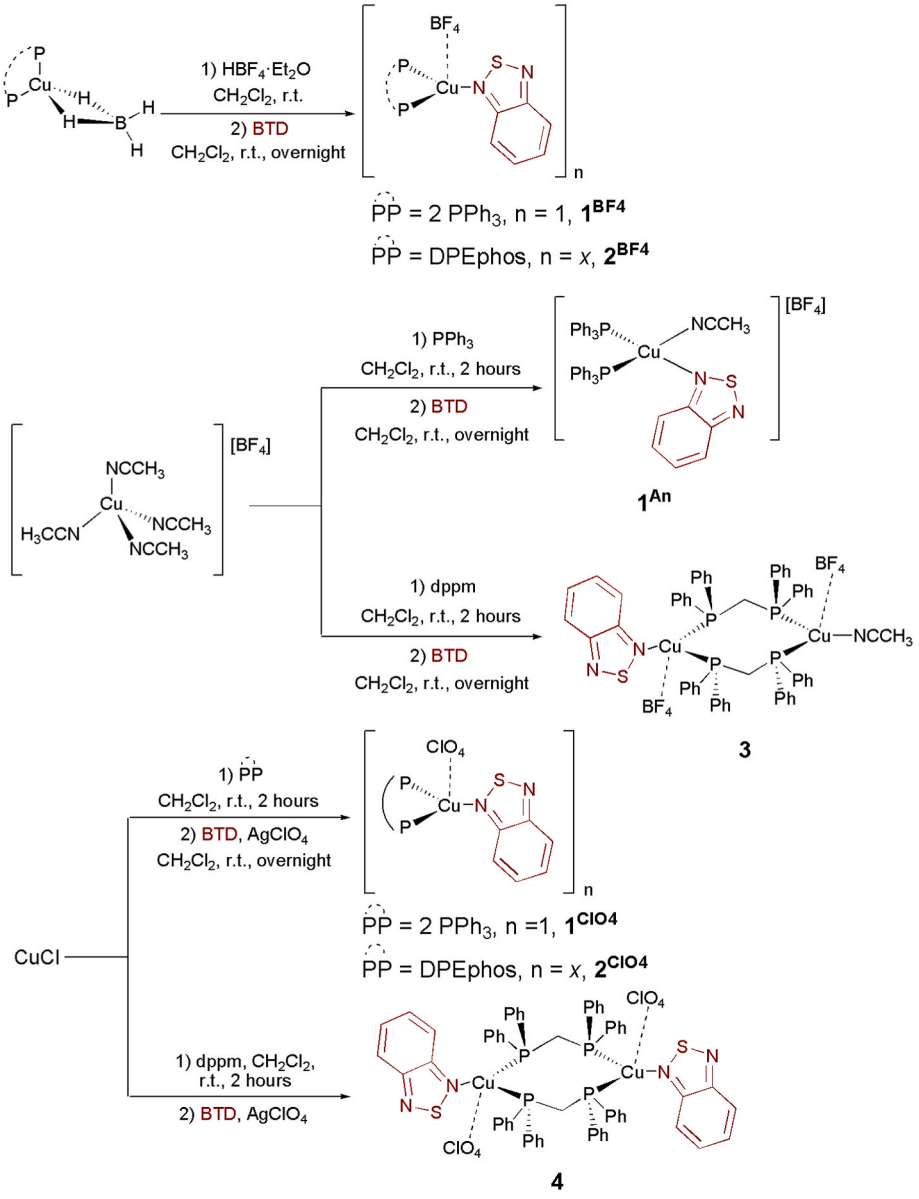

Scheme 1. Synthesis of heteroleptic 2,1,3-benzothiadiazole Cu(I) complexes.

1100-990 cm^{-1} range, as observable for instance in the IR spectra of $\mathbf{1}^{\mathbf{BF4}}$ and $\mathbf{1}^{\mathbf{ClO4}}$, superimposed in Fig. S1. No evidence of B–H bonds could be noticed for the complexes obtained from borohydride precursors. The presence of coordinated acetonitrile was revealed in the case of **3** by the weak $\nu_{C\equiv N}$ stretching at 2280 cm^{-1} (Fig. S2). The same stretching was unfortunately too weak to be detected in the case of $\mathbf{1}^{\mathbf{An}}$.

The signals attributable to coordinated BTD were observed in the high frequency region of the ^1H NMR spectra recorded at variable temperatures, together with the resonances of the phenyl substituents of the phosphines. Despite the coordination, the BTD ligand appeared symmetric, showing two multiplets in the high frequency region for all the complexes. Accordingly, only three BTD resonances were detected in the $^{13}C\{^1H\}$ NMR spectra. The ^1H and $^{13}C\{^1H\}$ NMR suggest fluxional behaviour in solution, as confirmed by the broadness of the $^{31}P\{^1H\}$ NMR spectra, composed by a single resonance also in the case of the asymmetric complex **3**. Resonances in the low frequency region were observed for complexes $\mathbf{1}^{\mathbf{An}}$, **3** and **4**, having acetonitrile and/or dppm in the coordination sphere. In particular, the methyl fragment of acetonitrile resonated respectively at 2.32 and 2.18 ppm in the ^1H NMR spectra of $\mathbf{1}^{\mathbf{An}}$ and **3**, with HSQC-correlated ^{13}C resonances at around 2.5 ppm. ^1H NMR, $^{31}P\{^1H\}$ NMR, $^{13}C\{^1H\}$ NMR and ^{13}C–^1H HSQC spectra of the complexes can be found in ESI together with IR spectra (Figs. S3–S15).

Electrochemical measurements were conducted on free BTD, $\mathbf{1}^{\mathbf{ClO4}}$ and $\mathbf{2}^{\mathbf{ClO4}}$ in acetone solutions with lithium perchlorate as supporting electrolyte (Fig. S16). Two irreversible oxidation processes occur for the free ligand around 1.2 and 1.7 V *vs* Fc/Fc^+, while irreversible reductions of BTD happen around −1.9 and −2.2 V *vs* Fc/Fc^+. The process at −1.9 V is associated to a reverse oxidation peak around −0.4 V. Complete cyclic voltammograms were collected only limiting the potential window to the first oxidation and reduction processes, since the expansion at higher or lower potentials caused the accumulation of decomposition products on the electrode surface. Roughly comparable processes are present also for the complexes, anticipated by irreversible oxidation peaks in the 0.6 − 0.9 V *vs* Fc/Fc^+ range, attributed to the $\{CuP_2\}$ fragment. As for the free ligand, the oxidations at higher potentials and the reduction processes caused the formation of decomposition products on the electrode surface, thus limiting the electrochemical investigation.

Given the fluxional behaviour in solution, the analytical and spectroscopic data do not unambiguously support the coordination environments proposed in Scheme 1. In the cases of $\mathbf{1}^{\mathbf{BF4}}$, $\mathbf{1}^{\mathbf{ClO4}}$ and **3** the solid-state structures were ascertained by means of single-crystal X-ray diffraction. Suitable crystals were isolated from dichloromethane/diethyl ether or from the slow evaporation of diethyl ether solutions. All three complexes crystallized in the monoclinic $P2_1/c$ (No. 14) space group.

In the solid state, the counteranion is incorporated into the coordination sphere of the metal through long interactions. As observable in Fig. 1, the copper atom in $\mathbf{1}^{\mathbf{BF4}}$ and $\mathbf{1}^{\mathbf{ClO4}}$ is bonded to two

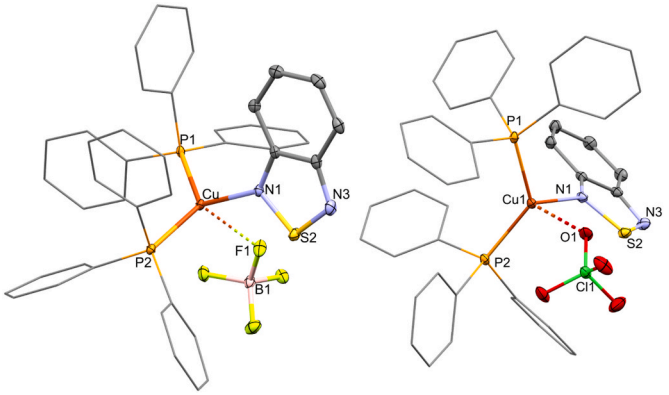

Fig. 1. Plots of $\mathbf{1}^{\mathbf{BF4}}$ and $\mathbf{1}^{\mathbf{ClO4}}$ (ellipsoids at 50% probability level). Hydrogen atoms are omitted for clarity.

triphenylphosphines and a BTD acting as a *N*-donor. Crystal data and structure refinement are set out in Table S1. Selected bond lengths and angles are collected in Table 1. Despite the soft Pearson characters of the Cu(I) centre and of the sulphur atom, BTD always coordinates through one of the nitrogen atoms [73–75].

For what concerns $\mathbf{1}^{\mathbf{BF4}}$, a first look at the complex suggests considering a trigonal planar coordination for Cu(I), related to the two PPh_3 and the BTD ligands. The copper atom is however not in the plane formed by the three donor atoms, but it is 0.3688(6) Å over the plane. Moreover, at only 2.3321(13) Å from the copper atom and at 2.503(2) Å from the plane there is a fluorine atom of BF_4^-. Although the Cu–F distance is longer than the sum of covalent radii, respectively equal to 1.32 (4) Å for Cu and 0.57(3) Å for F [99], the interaction could be considered as an example of the so-called coinage- (or regium-) bond [100] since it is shorter than the sum of the van der Waals radii [101]. Longer Cu–F distances respectively equal to 2.602(5) and 2.5232(2) Å were observed for instance for the mononuclear complex $[Cu(OH_2)(PPh_3)_2][BF_4]$ and for the 3,5-dimethylpyrazole ($HPzMe_2$) 2,20-bis(diphenylphosphino)-1, 10-bi-naphthyl (BINAP) complex $[Cu(HPzMe_2)(BINAP)][BF_4]$ [102, 103]. The Cu–F interaction is also shorter than those measured for several tetrafluoroborate salts of dinuclear and polynuclear Cu(I) complexes with phosphines and *N*-donor heterocycles in the coordination sphere [104–107]. The geometry around the copper atom in $\mathbf{1}^{\mathbf{BF4}}$ is therefore between a tetrahedron and a vacant trigonal bipyramid. Considering this last geometry, there is a plane defined by N(1), P(1) and P(2), and the fluorine atom is at one of the axial positions, while the other one is vacant. The basal triangular plane presents an important distortion since the expected angle of 120° increases up to 127.93(2)° for P–Cu–P perhaps because of the bulky substituents on the phosphorus atoms. It is worth noting that P–Cu–P angles have important influences on the photophysical properties of Cu(I) phosphine complexes [108, 109]. As shown in Fig. S17, the BTD position is not equidistant from the two phosphine ligands, and the N(1)-Cu-P(1) and N(1)-Cu-P(2) angles are respectively 118.67(5) and 104.98(5)°. The angle between the nine-membered BTD plane and the Cu–N vector is only 2.44(7)°, but the dihedral angle between the BTD plane and the basal N(1)-P(1)-P(2) plane is 60.47(4)°, so the BTD plane is inclined with respect to that plane. The BF_4^- position is also asymmetric with respect to the other ligands, with F(1)-Cu-P(1) and F(1)-Cu-P(2) angles respectively of 101.85(4) and 114.14(4)°.

For what concerns $\mathbf{1}^{\mathbf{ClO4}}$, the environment of the Cu(I) ion is similar to that of $\mathbf{1}^{\mathbf{BF4}}$ considering the change of the anion, but the geometry around Cu(I) is best defined as a distorted tetrahedron. The copper atom is situated at 0.4363(4) Å from the N(1)-P(1)-P(2) basal plane, while it

Table 1
Selected bond lengths [Å] and angles [°] for $\mathbf{1}^{\mathbf{BF4}}$ and $\mathbf{1}^{\mathbf{ClO4}}$.

1^{BF4}		1^{ClO4}		
Cu–N(1)	2.0940(17)	Cu(1)-N(1)	2.0945(11)	
Cu–P(1)	2.2488(5)	Cu(1)-P(1)	2.2497(4)	
Cu–P(2)	2.2686(6)	Cu(1)-P(2)	2.2799(4)	
Cu–F(1)	2.3321(13)	Cu(1)-O(1)	2.2513(11)	
N(1)-S(2)	1.6356(18)	N(1)-S(2)	1.6328(12)	
N(1)-C(9)	1.357(3)	N(1)-C(9)	1.3552(17)	
N(3)-S(2)	1.6060(19)	N(3)-S(2)	1.6116(12)	
N(3)-C(8)	1.346(3)	N(3)-C(8)	1.3467(18)	
B(1)-F(1)	1.412(3)	Cl(1)-O(1)	1.4553(11)	
B(1)-F(2)	1.392(3)	Cl(1)-O(2)	1.4182(11)	
B(1)-F(3)	1.389(3)	Cl(1)-O(3)	1.370(3)	1.525(5)
B(1)-F(4)	1.381(3)	Cl(1)-O(4)	1.518(4)	1.347(4)
N(1)-Cu-P(1)	118.67(5)	N(1)-Cu(1)-P(1)	113.65(3)	
N(1)-Cu-P(2)	104.98(5)	N(1)-Cu(1)-P(2)	104.57(3)	
P(1)-Cu-P(2)	127.93(2)	P(1)-Cu(1)-P(2)	130.008(14)	
N(1)-Cu-F(1)	78.29(6)	N(1)-Cu(1)-O(1)	86.57(5)	
P(1)-Cu-F(1)	101.85(4)	P(1)-Cu(1)-O(1)	104.49(4)	
P(2)-Cu-F(1)	114.14(4)	P(2)-Cu(1)-O(1)	108.89(3)	

was 0.367 Å for $\mathbf{1}^{\mathbf{BF4}}$. The fourth coordination position is occupied by an oxygen atom from the ClO_4^- anion situated at 2.2513(11) Å. This distance is shorter than the sum of the van der Waals radii [99–101], and also than the values found for instance in [Cu{2-(3′-pyridyl)benzoxazole}$(PPh_3)_2(OClO_3)$], 2.295(6) Å [110] and [Cu_2(dppm)$_2$(NCNMe$_2$)$_2(ClO_4)$][ClO_4], 2.323(5) and 2.329(5) Å [111]. It is noteworthy that the three bond angles around the metal centre defined by N(1), P(1) and P(2) are respectively 104.57(3), 113.65(3) and 130.01(1)°. The first two should be equal in a regular geometry, but they show in $\mathbf{1}^{\mathbf{ClO4}}$ an important difference. The P(1)-Cu-P(2) angle is even more obtuse than that found in $\mathbf{1}^{\mathbf{BF4}}$, and this could influence the photophysical properties [108,109]. Some tricoordinated [CuX$(PPh_3)_2$] complexes can be found in the literature with similar angles [112,113], as well as tetracoordinated derivatives [49]. From a structural point of view, it is interesting to observe the different coordination of the BTD ligand by comparing $\mathbf{1}^{\mathbf{BF4}}$ (Fig. S17) and $\mathbf{1}^{\mathbf{ClO4}}$ (Figs. S18–S19). In $\mathbf{1}^{\mathbf{ClO4}}$ the N–Cu vector is slightly bent, so that the BTD plane and the N–Cu bond form an angle of 14.03(6)°, while it was 2.44(7)° in $\mathbf{1}^{\mathbf{BF4}}$. This is possibly caused by the intermolecular π,π′-stacking interaction between the heterocyclic ring and phenyl ring, which facilitates the packing of two neighbouring monomers in a head-to-tail manner (see Fig. S20 and Table S2). The dihedral angle between the nine-membered BTD plane and the basal N(1)-P(1)-P(2) plane in $\mathbf{1}^{\mathbf{ClO4}}$ is 77.87(3)°, so the disposition is much more perpendicular if compared to $\mathbf{1}^{\mathbf{BF4}}$, where the same angle was 60.47(4)°.

The use of the bidentate phosphine dppm provided the dinuclear complex **3**, with two Cu(I) atoms asymmetrically coordinated, as observable in Fig. 2. Crystal data and structure refinement are set out in Table S3. Selected bond lengths and angles are given in Table 2. Cu(1) bears two phosphorus atoms from two different dppm ligands and one BTD acting as a *N*-donor, while Cu(2) is coordinated to the other two phosphorus atoms of dppm ligands and a nitrogen atom from an acetonitrile molecule. Both the copper atoms are tricoordinated in a planar trigonal geometry.

The sum of all the angles around Cu(1) is 358.7°, while it is 359.5° for Cu(2). Cu(1) and Cu(2) deviate from the corresponding planes formed by the three donor atoms respectively by 0.130(1) and 0.092(1) Å. The angles around the metal centres are quite different, since those concerning Cu(2) are close to 120°, while the coordination sphere around Cu(1) is much more distorted, with a P–Cu(1)-P angle of 152.43(4)° and P–Cu(1)-N angles of 99.3(1) and 106.9(1)°. The two copper atoms are arranged together by two dppm with the formation of a $Cu_2P_4C_2$ cyclic eight-membered framework. The distance between the metal centres is quite long, equal to 3.3135(7) Å [114]. There are about 175 compounds described in the CCDC database with two bridging dppm ligands joining two copper atoms [115], but only six examples show different environments for the two copper atoms as occurs for **3**. In most of the compounds described in the literature, the eight-membered ring $Cu_2P_4C_2$ is symmetrical and shows a chair-like conformation [116], although some examples of boat-like conformation were also reported [117]. The conformation of **3** (see Fig. S21) is quite abnormal because the carbon atoms of the eight-membered ring are both above the {P_4} plane (boat conformation) [118], but the Cu(I) atoms lie one below the plane by 1.040(1) Å, Cu(2), while the other one, Cu(1), is almost in the plane, separated only by 0.101(1) Å. BTD is coordinated to Cu(1), and the ligand occupies an equatorial position with N(1) only 0.148(4) Å below the {P_4} plane. The N(1)-Cu(1)-Cu(2) angle is therefore almost linear, being equal to 169.60(10)°. On the other hand, the CH_3CN ligand is in an axial conformation, N(2) atom is 2.963(4) Å below the {P_4} plane and the N(2)-Cu(2)-Cu(1) angle is almost perpendicular, 94.55(10)°. The acetonitrile molecule is linear, and the C–C–N and C–N–Cu angles of 178.6(4)° and 168.1(3)° show the usual behaviour exhibited by this ligand [117]. The plane of the BTD ligand does not bisect the P–Cu–P angle, and the angle between the nine-membered plane of the heterocycle and the N(1)-Cu(1) bond vector is 20.81(16)° (see Fig. S22).

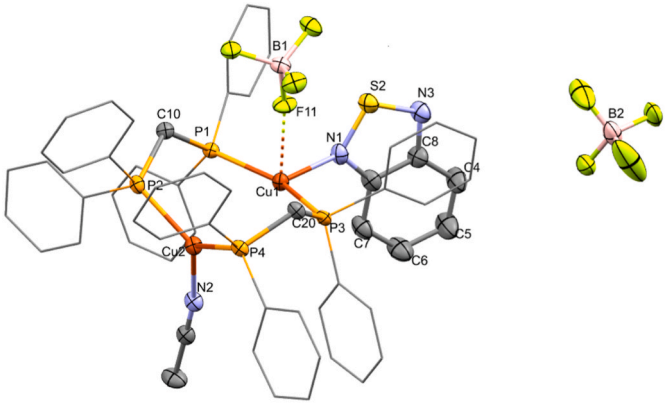

Fig. 2. Plot of **3** (ellipsoids at 50% probability level). Hydrogen atoms are omitted for clarity.

Table 2
Selected bond lengths [Å] and angles [°] for **3**.

Cu(1)-N(1)	2.089(3)	Cu(2)-N(2)	1.967(3)
Cu(1)-P(1)	2.2230(11)	Cu(2)-P(2)	2.2593(12)
Cu(1)-P(3)	2.2314(11)	Cu(2)-P(4)	2.2518(11)
Cu(1)-F(11)	2.541(2)	Cu(1)-Cu(2)	3.3135(7)
B(1)-F(11)	1.418(5)	B(2)-F(21)	1.381(7)
B(1)-F(12)	1.384(5)	B(2)-F(22)	1.385(6)
B(1)-F(13)	1.397(5)	B(2)-F(23)	1.372(7)
B(1)-F(14)	1.392(5)	B(2)-F(24)	1.376(7)
N(1)-S(2)	1.634(4)	S(2)-N(3)	1.605(4)
N(1)-C(9)	1.354(6)	N(3)-C(8)	1.356(6)
N(2)-C(1)	1.141(5)	C(1)-C(2)	1.457(6)
N(1)-Cu(1)-P(1)	106.89(10)	N(2)-Cu(2)-P(2)	117.31(11)
N(1)-Cu(1)-P(3)	99.34(10)	N(2)-Cu(2)-P(4)	120.65(11)
P(1)-Cu(1)-P(3)	152.43(4)	P(4)-Cu(2)-P(2)	121.50(4)
N(1)-Cu(1)-F(11)	89.33(12)	N(2)-Cu(2)-Cu(1)	94.55(10)
P(1)-Cu(1)-F(11)	86.81(7)	P(4)-Cu(2)-Cu(1)	91.58(3)
P(3)-Cu(1)-F(11)	85.11(7)	P(2)-Cu(2)-Cu(1)	91.26(3)
N(1)-Cu(1)-Cu(2)	169.60(10)	C(1)-N(2)-Cu(2)	168.1(3)
P(1)-Cu(1)-Cu(2)	77.94(3)	N(2)-C(1)-C(2)	178.6(4)
P(3)-Cu(1)-Cu(2)	77.64(3)		
F(11)-Cu(1)-Cu(2)	100.25(6)		

The asymmetric unit contains two tetrafluoroborate anions, one of them with a fluorine atom at 2.541(2) Å from Cu(1) and at 2.406(2) Å from the related P_2N plane. As described for $\mathbf{1}^{\mathbf{BF4}}$, the fluorine appears in the axial position of a vacant trigonal pyramid and the interaction can be considered another example of the so-called regium-bond. A comparable situation involves Cu(2), because a fluorine of a neighbour molecule with symmetry operation 0.5-x, y-0.5, 1.5-z is situated at 3.001(3) Å, but the distance to the P_2N plane is shorter and equal to 2.808(3) Å (see Fig. S23).

The nature of the bond between Cu(I) and BF_4^- or ClO_4^- was investigated for $\mathbf{1}^{\mathbf{BF4}}$ and $\mathbf{1}^{\mathbf{ClO4}}$ by means of *C*-PCM/MN15 DFT calculations. The presence of a continuous medium was introduced to avoid the overestimation of electrostatic interactions between cations and anions. The AIM analysis revealed in the case of the model structure of $\mathbf{1}^{\mathbf{BF4}}$ the presence of two (3,-1) bond critical points (BCP) between the metal centre and two fluorine atoms of the counterion (see Fig. 3). Selected computed properties at BCP are reported in Table 3. The electron density (ρ) and potential energy density (V) values indicate that the two Cu···F interactions have different strengths. The energy density (E) and Laplacian of electron density ($\nabla^2\rho$) give information about the nature of the interactions. In particular, the negative sign of E and the positive value of $\nabla^2\rho$ are in agreement with Bianchi's definition of dative bond [119–121]. The AIM analyses revealed a quite different interaction with the counterion in the case of the DFT-optimized structure of $\mathbf{1}^{\mathbf{ClO4}}$. As

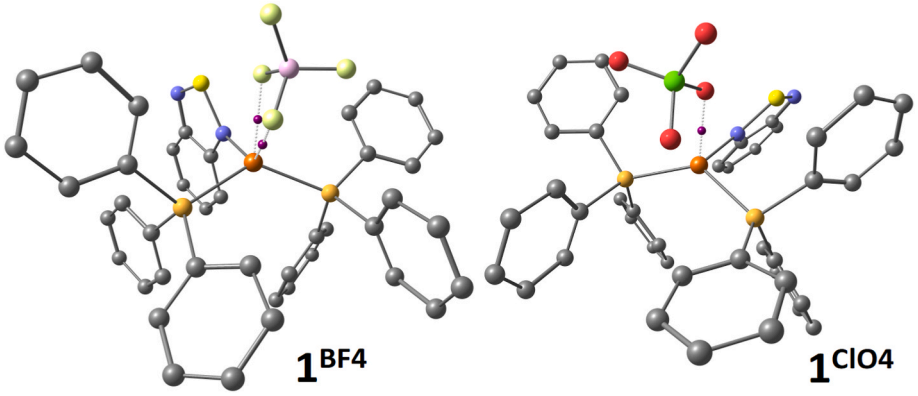

Fig. 3. DFT-optimized structures of $\mathbf{1}^{\mathbf{BF4}}$ and $\mathbf{1}^{\mathbf{ClO4}}$ (*C*-PCM/MN15/def2-SVP). Colour map: Cu, orange; Cl, green; S, yellow; P, light orange; F; greenish yellow; O, red; N, blue; C, grey; B, pink. Hydrogen atoms are omitted for clarity. Selected (3,-1) BCPs as small purple spheres.

Table 3
Selected properties at Cu···F and Cu···O (3,-1) BCPs for the DFT-optimized structures of $\mathbf{1}^{\mathbf{BF4}}$ and $\mathbf{1}^{\mathbf{ClO4}}$. ρ = electron density, e Å^{-3}; V = potential energy density, Hartree Å^{-3}; E = energy density, Hartree Å^{-3}; $\nabla^2\rho$ = Laplacian of electron density, e Å^{-5}.

	Cu···F [Å]	ρ	V	E	$\nabla^2\rho$
$\mathbf{1}^{\mathbf{BF4}}$	2.518	0.148	−0.175	−0.027	1.663
	2.345	0.202	−0.250	−0.020	2.940
	Cu···O [Å]	**ρ**	**V**	**E**	**$\nabla^2\rho$**
$\mathbf{1}^{\mathbf{ClO4}}$	2.194	0.310	−0.391	0.196	6.097

observable in Fig. 3, only one Cu···O (3,-1) BCP was localized. The positive values of both E and $\nabla^2\rho$ (Table 3) are in line with an electrostatic interaction.

The structure proposed for $\mathbf{1}^{\mathbf{An}}$ in Scheme 1, [Cu(NCCH$_3$)(BTD)(PPh$_3$)$_2$][BF$_4$], was computationally optimized and compared with possible isomers, in particular [Cu(BF$_4$)(BTD)(PPh$_3$)]•••CH$_3$CN and [Cu(BF$_4$)(NCCH$_3$)(PPh$_3$)]•••BTD. As observable in Fig. S24, the isomer with {N$_2$P$_2$} inner coordination sphere was the most stable, even if the Gibbs energy difference with the other species is limited, indicating the roughly comparable coordinating ability of CH$_3$CN, BTD and the BF_4^- anion.

For what concerns $\mathbf{2}^{\mathbf{BF4}}$ and $\mathbf{2}^{\mathbf{ClO4}}$, mononuclear geometries in line with those experimentally observed for $\mathbf{1}^{\mathbf{BF4}}$ and $\mathbf{1}^{\mathbf{ClO4}}$ were optimized and compared with dinuclear derivatives having formulae [Cu(DPEphos)(BF$_4$)(μ-BTD)Cu(BTD)(DPEphos)][BF$_4$] and [Cu(DPEphos)(ClO$_4$)(μ-BTD)Cu(BTD)(DPEphos)][ClO$_4$], trying to take into account the possible formation of coordination polymers. The optimized geometries are shown in Fig. S25 with the relative energy values. The dinuclear models revealed to be strictly comparable to the mononuclear counterparts from a thermodynamic point of view, thus suggesting that the DPEphos derivatives could be polynuclear compounds.

Finally, in the case of compound **4**, DFT calculations afforded a stationary point in line with the experimental structure of **3**, *i.e.* a dinuclear geometry with bridging dppm ligands and ClO_4^- ions interacting with the Cu(I) centres (computed Cu–O distances 2.168 and 2.330 Å). The DFT-optimized structure of **4** is shown in Fig. S26.

3.2. Absorption and emission features

The complexes are characterized by absorptions for wavelengths below 375 nm in diluted CH_2Cl_2 solutions (see Figs. S27 and S28), roughly coincident with the $\pi^*\leftarrow\pi$ transitions of free BTD at longer wavelengths. Although the complexes are yellow or orange powders at the solid state, once dissolved in common organic solvents the colour disappears and no tail in the visible range is observable. As a consequence, solution of the complexes at the concentrations typical of conductivity measurements and UV–Vis spectroscopy are colourless. The extension of the absorption range, most likely accountable to MLCT transitions, can be detected at the solid state, with absorptions in the violet-blue region (see the inset of Fig. S27). The different transitions observed passing from solid state to solution agree with the fluxional behaviour previously deducted by means of NMR spectroscopy. In fact, according to the X-ray structures previously discussed, four different ^{1}H NMR aromatic resonances are expected for BTD acting as monodentate ligand, and not only two as experimentally observed. The reversible dissociation of BTD probably accounts for the lack of charge transfer absorptions in solution. Moreover, it is worth noting that the photophysical properties of low-coordinated Cu(I), Ag(I) and Au(I) metal complexes are very sensitive to subtle anion contacts because of the resulting structural distortions both at the ground and at the excited state [122–127].

TD-DFT calculations were conducted on the computed structures of $\mathbf{1}^{\mathbf{BF4}}$ and $\mathbf{1}^{\mathbf{ClO4}}$. The hole and electron distributions associated with the singlet-singlet transition, depicted in Fig. 4, clearly indicate that the lowest-energy absorptions have a charge transfer nature, with the electron moving from an occupied orbital centred on the metal centre and on the *P*-donors to an unoccupied π* orbital of the BTD ligand. The molecular orbitals mostly involved in the processes are HOMO and LUMO, as deducible from Table S4, even if the contribution of other occupied orbitals is not negligible. The HOMOs are mostly localized of the {CuP$_2$} fragment and on the *P*-bonded aryl substituents, while the LUMOs coincide with a π* orbital of the BTD heterocycle (Fig. S29).

Excitation of powder samples with near-UV and violet-blue light affords intense red emissions centred between 620 and 685 nm. As expected from the absorption data, the luminescence is not maintained in solution, since the reversible break of the Cu-BTD bonds avoids the possibility of charge-transfer phenomena. Moreover, the dissociation of the counterions in solution could also play a role. A recent example is provided by the work of Ganter, Steffen and co-workers, that observed luminescence for *N*-heterocyclic carbene (NHC) Cu(I) complexes bearing pyridine derivatives (py^R) as chromophore ligands only when Cu–F interactions between BF_4^- and [Cu(py^R)(NHC)]$^+$ were present [128]. Photophysical data for all the complexes are summarized in Table 4, while the PL spectra collected with $\lambda_{excitation}$ = 350 nm are shown in Fig. 5. The excitation range of all the compounds covers the UV and part of the visible range, with an extension to longer wavelengths for the compounds with the most red-shifted emission maxima. The PLE spectra ($\lambda_{emission}$ = 630 nm) are collected in Fig. S30. The replacement of triphenylphosphines with DPEphos causes a red shift of the emission, as already observed for other Cu(I) derivatives [70]. The reduction of Φ appears almost in part related to the energy gap law [129,130]. The substitution of the tetrafluoroborate ion with perchlorate also shifts the emission towards longer wavelengths and reduces the Φ values,

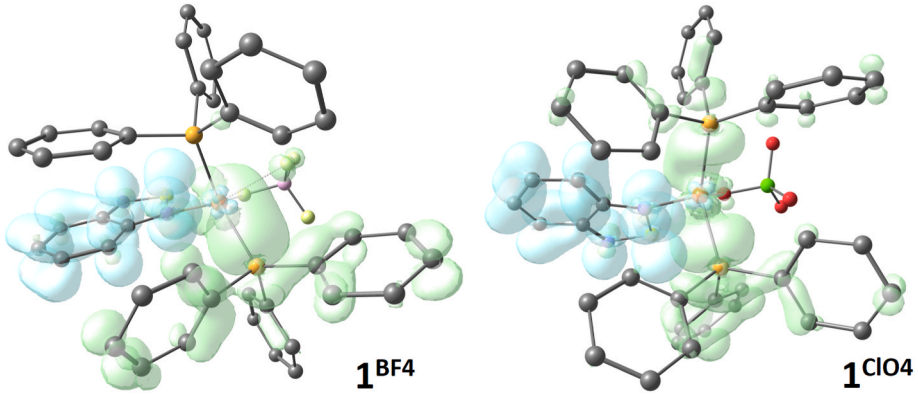

Fig. 4. DFT-optimized structures (ground singlet state) of $\mathbf{1}^{\mathbf{BF4}}$ and $\mathbf{1}^{\mathbf{ClO4}}$ with hole (green) and electron (cyan) distribution related to the lowest energy singlet←singlet absorption (surface isovalue = 0.001 a.u.). Colour map: Cu, orange; Cl, green; S, yellow; P, light orange; F; greenish yellow; O, red; N, blue; C, grey; B, pink. Hydrogen atoms are omitted for clarity.

Table 4
Photophysical data of the complexes at the solid state (r.t.).

	[a] PL, nm (FWHM: cm^{-1})	[b] PLE, nm	[c] τ, μs	[d] Φ, %
$\mathbf{1}^{\mathbf{BF4}}$	646 (FWHM = 3400)	<530	1310	46
$\mathbf{2}^{\mathbf{BF4}}$	675 (FWHM = 3400)	<590	70	31
$\mathbf{1}^{\mathbf{An}}$	638 (FWHM = 3100)	<520	1242	18
3	623 (FWHM = 3500)	<480	1789	35
$\mathbf{1}^{\mathbf{ClO4}}$	660 (FWHM = 3600)	<530	1572	38
$\mathbf{2}^{\mathbf{ClO4}}$	680 (FWHM = 3400)	<590	81	26
4	683 (FWHM = 4000)	<590	1283	13

[a] $\lambda_{excitation}$ = 350 nm.
[b] $\lambda_{emission}$ = 630 nm.
[c] $\lambda_{excitation}$ = 290 nm.
[d] $\lambda_{excitation}$ = 365 nm.

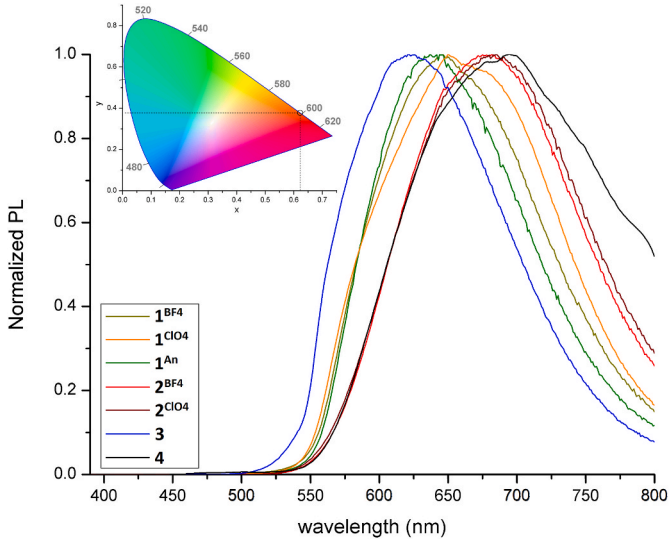

Fig. 5. Normalized PL spectra of the complexes and CIE 1931 diagram for $\mathbf{1}^{\mathbf{BF4}}$. Powder samples, r.t., $\lambda_{excitation}$ = 350 nm.

according to the non-innocent role of the counterions revealed by X-ray structures and DFT calculations. On comparing $\mathbf{1}^{\mathbf{BF4}}$ and $\mathbf{1}^{\mathbf{An}}$, the addition of an acetonitrile molecule in the Cu(I) coordination sphere poorly affects the emission maximum, but the Φ value of $\mathbf{1}^{\mathbf{An}}$ is meaningfully lower. Possible reasons are the vibrational coupling with the acetonitrile bonds and the change of Cu(I) geometry. For what concerns the dppm complexes **3** and **4**, the formal replacement of an acetonitrile ligand with BTD and the variation of counteranion from BF_4^- to ClO_4^- caused a red-shift of the emission maximum by about 60 nm, and the photoluminescence quantum yield of **3** is noticeably higher than that of **4**. It is likely to suppose that the modifications affected also the intermolecular interactions at the solid state, and it is not possible to rationalize the changes that occurred on the basis of the available data.

On considering the data reported in Table 4, the best performances in terms of Φ were achieved with the mononuclear triphenylphosphine derivative $\mathbf{1}^{\mathbf{BF4}}$ (46%). The CIE chromaticity coordinates are $x = 0.622$ and $y = 0.378$, corresponding to a reddish-orange emission with unitary colour purity (Fig. 5) [131]. The CIE 1931 region is the same as common Eu(III) luminescent derivatives [132–136], even if the observed colour for $\mathbf{1}^{\mathbf{BF4}}$ is more orange-shifted. The good photoluminescence quantum yields of the triphenylphosphine derivatives $\mathbf{1}^{\mathbf{BF4}}$ and $\mathbf{1}^{\mathbf{ClO4}}$ can be tentatively ascribed to the very large P–Cu–P angle, around 130°, as observed in similar compounds [49,56,137].

The Stokes shifts in the 5000–9000 cm^{-1} range (measured between the PL and the lowest energy PLE maxima) and the wide bands (FWHM values between 3000 and 4000 cm^{-1}) suggest the involvement of triplet excited states in the emission. This hypothesis is strongly supported by the observed lifetimes τ, that are in the micro- and millisecond ranges. It is worth noting that milliseconds-long lifetimes were reported only in a few cases for Cu(I) complexes at room temperature [138,139]. The choice of the phosphine strongly influences the observed lifetime, since DPEphos derivatives are characterized by much shorter τ values (tens of μs) if compared to triphenylphosphine and dppm complexes (thousands of μs). Such a difference can be tentatively attributed to different molecular structures, mononuclear for the triphenylphosphine complexes, and perhaps polynuclear with bridging BTD for the DPEphos-containing compounds.

In order to investigate the emission mechanism, TD-DFT simulations using the triplet ground state geometries of $\mathbf{1}^{\mathbf{BF4}}$ and $\mathbf{1}^{\mathbf{ClO4}}$ were carried out. The charge density differences associated with the lowest-energy triplet←singlet absorptions, *i.e.* the reverse processes of the phosphorescent emissions, are shown in Fig. 6. The plots show that the transitions involve the metal centre, the phosphine ligands and the occupied and empty orbitals of BTD. Table S4 reports selected predicted parameters for the transitions. As for the singlet ground state geometries, the frontier orbitals are principally involved, comparable to those described for the ground singlet states (Fig. S31).

The comparisons of $\mathbf{1}^{\mathbf{BF4}}$ with $\mathbf{1}^{\mathbf{ClO4}}$ and of $\mathbf{2}^{\mathbf{BF4}}$ with $\mathbf{2}^{\mathbf{ClO4}}$ highlight that the lifetimes are influenced by the choice of the counterion. The τ values are around 15% longer for perchlorates if compared to tetrafluoroborate salts, as highlighted in Fig. 7. The photoluminescence quantum yields are lower in the case of perchlorate derivatives, indicating that different alterations of the Cu(I) coordination sphere by the counterions influence the radiative kinetic constant. The values of the radiative (k_r) and non-radiative (k_{nr}) constants were estimated on the

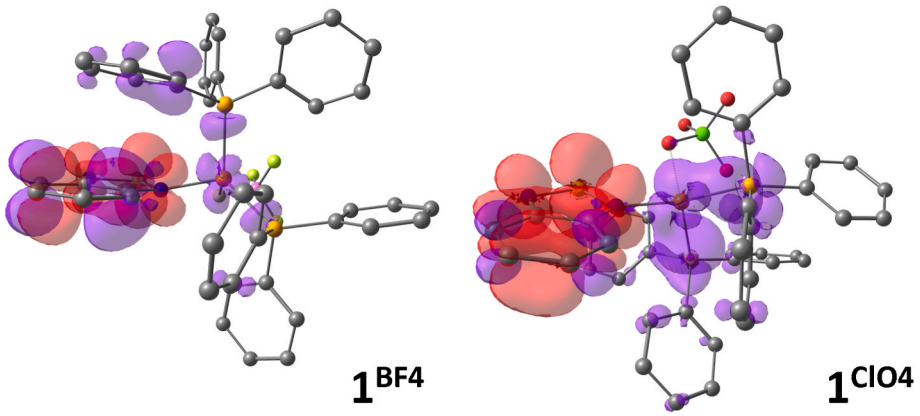

Fig. 6. DFT-optimized structures (triplet state) of $\mathbf{1}^{\mathbf{BF4}}$ and $\mathbf{1}^{\mathbf{ClO4}}$ with plots of the charge density difference (violet and red, surface isovalue = 0.001 a.u.) related to the lowest energy triplet←singlet absorption (the emission is the reverse process). Colour map: Cu, orange; Cl, green; S, yellow; P, light orange; F; greenish yellow; O, red; N, blue; C, grey; B, pink. Hydrogen atoms are omitted for clarity.

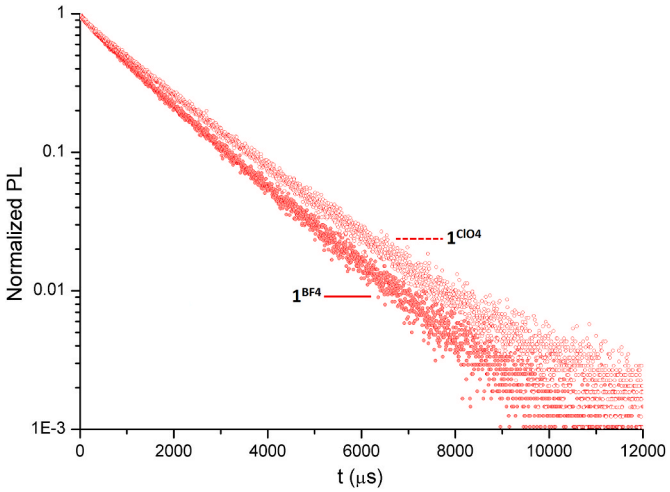

Fig. 7. Semi-log plot of luminescence decay curves of $\mathbf{1}^{\mathbf{BF4}}$ (full circles) and $\mathbf{1}^{\mathbf{ClO4}}$ (open circles). Powder samples, r.t., $\lambda_{excitation}$ = 290 nm, $\lambda_{emission}$ = 640–670 nm.

basis of the equation $\Phi = k_r/(k_r + k_{nr}) = \tau\ k_r$ and are summarized in Table S5 [140]. In the case of $\mathbf{1}^{\mathbf{BF4}}$ the k_r and k_{nr} values are respectively around $3.5\bullet10^2$ and $4.1\bullet10^2\ s^{-1}$. The k_r value in $\mathbf{1}^{\mathbf{ClO4}}$ is lower, $2.4\bullet10^2\ s^{-1}$, while the k_{nr} constant is comparable, $3.9\bullet10^2\ s^{-1}$. Similar considerations can be drawn from the comparison of $\mathbf{2}^{\mathbf{BF4}}$ and $\mathbf{2}^{\mathbf{ClO4}}$. The radiative constants are $4.4\bullet10^3$ and $3.2\bullet10^3\ s^{-1}$ respectively for the tetrafluoroborate and perchlorate derivatives, while the k_{nr} values are more similar, $9.9\bullet10^3\ s^{-1}$ for $\mathbf{2}^{\mathbf{BF4}}$ and $9.1\bullet10^3\ s^{-1}$ for $\mathbf{2}^{\mathbf{ClO4}}$.

The data provided indicate that the nature of the counterion mostly affects the k_r values. On considering the X-ray structures of $\mathbf{1}^{\mathbf{BF4}}$ and $\mathbf{1}^{\mathbf{ClO4}}$, the buried volume ($V\%_{bur}$) [98] values associated with tetrafluoroborate and perchlorate are respectively 25.5% (*z* axis along Cu···B) and 24.6% (*z* axis along Cu···Cl), while those of the ligands are 29.1–29.4% (BTD, *z* axis along Cu–N) and 63.2–62.8% (triphenylphosphines, *z* axis along Cu–N). Globally, $V\%_{bur}$ varies from 93.5% in $\mathbf{1}^{\mathbf{BF4}}$ to 92.5% in $\mathbf{1}^{\mathbf{ClO4}}$ (*z* axis along Cu–N). Since the influence of the coordinated ligands on the photoluminescence quantum yield is often discussed in the current literature in terms of $V\%_{bur}$ (with higher $V\%_{bur}$ commonly associated with a higher photoluminescence quantum yield) [63,141], the greater k_r value of $\mathbf{1}^{\mathbf{BF4}}$ is perhaps in some way related to the higher steric hindrance on the Cu(I) metal centre. The buried volumes are represented in Fig. S32. Another factor to be considered is the different nature of the Cu···BF_4 and Cu···ClO_4 interactions highlighted by AIM calculations, dative in the first case and electrostatic in the second one.

All these considerations should be extended to the long-living triplet states of the complexes, having different equilibrium geometries with respect to the singlet ground states. Recent findings on the influence of different counterions on the luminescence features of cationic Cu(I) complexes having formulae $[Cu(P\hat{c}P)(N\hat{c}N)]^+$ (P̂cP = oxydi(2,1-phenylene)bis(diphenylphosphane) and 9,9-dimethyl-9H-xanthene-4,5-diyl)bis(diphenylphosphane); N̂cN = 6-methyl-2,2′-bipyridine and 6,6′-dimethyl-2,2′-bipyridine) [125,126] suggest as possible explanation that the different environments surrounding the copper centre cause a variation of its charge density, thus leading to a change in the probability of spontaneous radiative decay. The Hirshfeld population analysis on $\mathbf{1}^{\mathbf{BF4}}$ and $\mathbf{1}^{\mathbf{ClO4}}$ in their triplet state geometries effectively evidenced a meaningful change of the copper partial charge, equal to 0.207 a.u. in $\mathbf{1}^{\mathbf{BF4}}$ and to 0.281 a.u. in $\mathbf{1}^{\mathbf{ClO4}}$.

4. Conclusions

The luminescent Cu(I) BTD complexes with formally unsaturated coordination spheres here reported revealed to have photophysical properties strongly dependent upon the choice of the ancillary ligands and the counterion. The non-innocent counterions generate interactions of different nature with the metal centre and alter the steric hindrance around Cu(I). The data collected suggest high adjustability of the luminescent features in this class of compounds on changing the coordination sphere, of potential interest for further developments. BTD itself can be functionalized and used as building block for the preparation of chelating ligands. The extremely long lifetimes and the wide excitation spectra of the reported compounds suggest possible future applications in photocatalysts. Moreover, some selected emission features roughly comparable to those of Eu(III) complexes make the Cu(I) BTD derivatives appealing in fields such as optoelectronics, anti-counterfeiting and data encryption.

CRediT authorship contribution statement

Valentina Ferraro: Conceptualization, Investigation, Formal analysis, Validation, Writing – original draft, Writing – review & editing. **Matteo Girotto:** Investigation, Formal analysis. **Jesús Castro:** Investigation, Formal analysis, Writing – original draft, Writing – review & editing. **Marco Bortoluzzi:** Conceptualization, Investigation, Formal analysis, Validation, Resources, Supervision, Funding acquisition, Writing – original draft, Writing – review & editing.

Declaration of competing interest

The authors declare that they have no known competing financial interests or personal relationships that could have appeared to influence the work reported in this paper.

Data availability

Data will be made available on request.

Acknowledgements

Università Ca' Foscari Venezia is gratefully acknowledged for financial support (Bando Spin 2018, D. R. 1065/2018 prot. 67416). CACTI (University of Vigo) and CINECA (Bologna) are respectively acknowledged for X-ray data collection and the availability of high performances computers resources (class C project COLUMN21, COLUMN22 and INLIGHT). This work is part of the "Network 4 Energy Sustainable Transition - NEST" project (MIUR project code PE000021, Concession Degree No. 1561 of October 11, 2022), in the framework of the NextGenerationEu PNRR plan (CUP C93C22005230007).

Appendix A. Supplementary data

Supplementary data to this article can be found online at https://doi.org/10.1016/j.dyepig.2023.111388.

References

[1] Neto BAD, Lapis AAM, da Silva. EN, dupont J. 2,1,3-Benzothiadiazole and derivatives: synthesis, properties, reactions, and applications in light technology of small molecules. Chem Eur J 2013:228–55. https://doi.org/10.1002/ejoc.201201161.
[2] Wu Y, Zhu W. Organic sensitizers from D–π–A to D–A–π–A: effect of the internal electron-withdrawing units on molecular absorption, energy levels and photovoltaic performances. Chem Soc Rev 2013;42:2039–58. https://doi.org/10.1039/C2CS35346F.
[3] Du J, Biewer MC, Stefan MC. Benzothiadiazole building units in solution-processable small molecules for organic photovoltaics. J Mater Chem 2016;4:15771–87. https://doi.org/10.1039/C6TA06241E.
[4] Wang Y, Michinobu T. Benzothiadiazole and its π-extended, heteroannulated derivatives: useful acceptor building blocks for high-performance donor–acceptor polymers in organic electronics. J Mater Chem C 2016;4:6200–14. https://doi.org/10.1039/C6TC01860B.
[5] Tan SE, Sarjadi MS. The recent development of carbazole-, benzothiadiazole-, and isoindigo-based copolymers for solar cells application: a review. Polym Sci B 2017;59:479–96. https://doi.org/10.1134/S1560090417050141.
[6] Zhao X, Chaudhry ST, Mei J. Chapter five - heterocyclic building blocks for organic semiconductors. Adv Heterocycl Chem 2017;121:133–71. https://doi.org/10.1016/bs.aihch.2016.04.009.
[7] Nakabayashi K, Takahashi T, Sugawara R, Lo C-T, Mori H. Benzothiadiazole-based donor–acceptor nanoparticles with solvatochromic and thermoresponsive properties. React Funct Polym 2018;131:350–60. https://doi.org/10.1016/j.reactfunctpolym.2018.08.011.
[8] Benevides TO, Regis E, Nicoleti CR, Bechtold IH, Vieira AA. Phase-dependent photoluminescence of non-symmetric 2,1,3-benzothiadiazole liquid crystals. Dyes Pigments 2019;163:300–7. https://doi.org/10.1016/j.dyepig.2018.12.012.
[9] Paczkowski IM, Coelho FL, Campo LF. 2,1,3-Benzothiadiazole dyes conjugated with benzothiazole and benzoxazole: synthesis, solvatochromism and solid-state properties. J Mol Liq 2020;319:114277. https://doi.org/10.1016/j.molliq.2020.114277.
[10] Zhang Y, Song J, Qu J, Qian P-C, Wong W-Y. Recent progress of electronic materials based on 2,1,3-benzothiadiazole and its derivatives: synthesis and their application in organic light-emitting diodes. Sci China Chem 2021;64:341–57. https://doi.org/10.1007/s11426-020-9901-4.
[11] Wang C, Liu F, Chen Q-M, Xiao C-Y, Wu Y-G, Li W-W. Benzothiadiazole-based conjugated polymers for organic solar cells. Chin J Polym Sci 2021;39:525. https://doi.org/10.1007/s10118-021-2537-8.
[12] Langis-Barsetti S, Maris T, Wuest JD. Molecular organization of 2,1,3-benzothiadiazoles in the solid state. J Org Chem 2017;82:5034–45. https://doi.org/10.1021/acs.joc.6b02778.
[13] Ho PC, Wang JZ, Meloni F, Vargas-Baca I. Chalcogen bonding in materials chemistry. Coord Chem Rev 2020;422:213464. https://doi.org/10.1016/j.ccr.2020.213464.
[14] Toscani A, Marín-Hernández C, Moragues ME, Sancenón F, Dingwall P, Brown NJ, Martínez-Máñez R, White AJP, Wilton-Ely JDET. Ruthenium(II) and osmium(II) vinyl complexes as highly sensitive and selective chromogenic and fluorogenic probes for the sensing of carbon monoxide in air. Chem Eur J 2015;21:14529–38. https://doi.org/10.1002/chem.201501843.
[15] de la Torre C, Toscani A, Marín-Hernández C, Robson JA, Terencio MC, White AJP, Alcaraz MJ, Wilton-Ely JDET, Martínez-Máñez R, Sancenón F. *Ex vivo* tracking of endogenous CO with a ruthenium(II) complex. J Am Chem Soc 2017;139:18484–7. https://doi.org/10.1021/jacs.7b11158.
[16] Sukhikh TS, Ogienko DS, Bashirov DA, Konchenko SN. Luminescent complexes of 2,1,3-benzothiadiazole derivatives. Russ Chem Bull Int Ed 2019;68:651–61. https://doi.org/10.1007/s11172-019-2472-9.
[17] Toscani A, Marín-Hernández C, Robson JA, Chua E, Dingwall P, White AJP, Sancenón F, de la Torre C, Martínez-Máñez R, Wilton-Ely JDET. Highly sensitive and selective molecular probes for chromo-fluorogenic sensing of carbon monoxide in air, aqueous solution and cells. Chem Eur J 2019;25:2069–81. https://doi.org/10.1002/chem.201805244.
[18] Kuznetsova A, Matveevskaya V, Pavlov D, Yakunenkov A, Potapov A. Coordination polymers based on highly emissive ligands: synthesis and functional properties. Materials 2020;13:2699. https://doi.org/10.3390/ma13122699.
[19] Robson JA, Kubánková M, Bond T, Hendley RA, White AJP, Kuimova MK, Wilton-Ely JDET. Simultaneous detection of carbon monoxide and viscosity changes in cells. Angew Chem Int Ed 2020;59:21431–5. https://doi.org/10.1002/anie.202008224.
[20] Khisamov R, Sukhikh T, Bashirov D, Ryadun A, Konchenko S. Structural and photophysical properties of 2,1,3-benzothiadiazole-based phosph(III)azane and its complexes. Molecules 2020;25:2428. https://doi.org/10.3390/molecules25102428.
[21] Khisamov RM, Ryadun AA, Konchenko SN, Sukhikh TS. Fluorescence vs. Phosphorescence: which scenario is preferable in Au(I) complexes with benzothiadiazoles. Molecules 2022;27:8162. https://doi.org/10.3390/molecules27238162.
[22] Volz D, Wallesch M, Fléchon C, Danz M, Verma A, Navarro JM, Zink DM, Bräse S, Baumann T. From iridium and platinum to copper and carbon: new avenues for more sustainability in organic light-emitting diodes. Green Chem 2015;17:1988–2011. https://doi.org/10.1039/C4GC02195A.
[23] Bizzarri C, Spuling E, Knoll DM, Volz D, Bräse S. Sustainable metal complexes for organic light-emitting diodes (OLEDs). Coord Chem Rev 2018;373:49–82. https://doi.org/10.1016/j.ccr.2017.09.011.
[24] Wenger OS. Photoactive complexes with earth-abundant metals. J Am Chem Soc 2018;140:13522–33. https://doi.org/10.1021/jacs.8b08822.
[25] Zhang Y, Schulz M, Wächtler M, Karnahl M, Dietzek B. Heteroleptic diimine–diphosphine Cu(I) complexes as an alternative towards noble-metal based photosensitizers: design strategies, photophysical properties and perspective applications. Coord Chem Rev 2018;356:127–46. https://doi.org/10.1016/j.ccr.2017.10.016.
[26] Förster C, Heize K. Photophysics and photochemistry with Earth-abundant metals – fundamentals and concepts. Chem Soc Rev 2020;49:1057–70. https://doi.org/10.1039/c9cs00573k.
[27] Wegeberg C, Wenger OS. Luminescent first-row transition metal complexes. JACS Au 2021;1:1860–76. https://doi.org/10.1021/jacsau.1c00353.
[28] Li X, Xie Y, Li Z. Diversity of luminescent metal complexes in OLEDs: beyond traditional precious metals. Chem Asian J 2021;16:2817–29. https://doi.org/10.1002/asia.202100784.
[29] Cavinato LM, Wölfl S, Pöthig A, Fresta E, Garino C, Fernandez-Cestau J, Barolo C, Costa RD. Multivariate analysis identifying $[Cu(N\check{C}N)(P\check{C}P)]^+$ design and device architecture enables first-class blue and white light-emitting electrochemical cells. Adv Mater 2022;34:2109228. https://doi.org/10.1002/adma.202109228.
[30] Takeda H, Kobayashi A, Tsug K. Recent developments of photoactive Cu(I) and Ag(I) complexes with diphosphine and related ligands. Coord Chem Rev 2022;470:214700. https://doi.org/10.1016/j.ccr.2022.214700.
[31] Beaudelot J, Oger S, Peruško S, Phan T-A, Teunens T, Moucheron C, Evano G. Photoactive copper complexes: properties and applications. Chem Rev 2022;122:16365–609. https://doi.org/10.1021/acs.chemrev.2c00033.
[32] Mejía E, Luo SP, Karnahl M, Friedrich A, Tschierlei S, Surkus AE, Junge H, Gladiali S, Lochbrunner S, Beller M. A noble-metal-free system for photocatalytic hydrogen production from water. Chem Eur J 2013;19:15972–8. https://doi.org/10.1002/chem.201302091.
[33] Xu L-X, Wang T-Q, Liu X-F, Chen H, Wei C-J, Xu DD, Chen F, Li Y, Luo S-P. The heteroleptic Cu(I) photosensitizer-containing 3,8-disubstituted phenanthroline: synthesis, photophysical properties and photocatalytic hydrogen evolution from water. Eur J Inorg Chem 2020:4278–83. https://doi.org/10.1002/ejic.202000648.
[34] Forero Cortés PA, Marx M, Trose M, Beller M. Heteroleptic copper complexes with nitrogen and phosphorus ligands in photocatalysis: overview and perspectives. Chem Catal 2021;1:298–338. https://doi.org/10.1016/j.checat.2021.05.005.
[35] Bizzarri C. Homogeneous systems containing earth-abundant metal complexes for photoactivated CO_2 reduction: recent advances. Eur J Org Chem 2022:e202200185. https://doi.org/10.1002/ejoc.202200185.
[36] Scaltrito DV, Thompson DW, O'Callaghan JA, Meyer GJ. MLCT excited states of cuprous bis-phenanthroline coordination compounds. Coord Chem Rev 2000;208:243–66. https://doi.org/10.1016/S0010-8545(00)00309-X.
[37] Lavie-Cambot A, Cantuel M, Leydet Y, Jonusauskas G, Bassani DM, McClenaghan ND. Improving the photophysical properties of copper(I) bis(phenanthroline) complexes. Coord Chem Rev 2008;252:2572–84. https://doi.org/10.1016/j.ccr.2008.03.013.
[38] Tsubomura T, Kimura K, Nishikawa M, Tsukuda T. Structures and photophysical properties of copper(I) complexes bearing diphenylphenanthroline and bis

(diphenylphosphino)alkane: the effect of phenyl groups on the phenanthroline ligand. Dalton Trans 2015;44:7554–62. https://doi.org/10.1039/C5DT00835B.
[39] Keller S, Pertegás A, Longo G, Martínez L, Cerdá J, Junquera-Hernández JM, Prescimone A, Constable EC, Housecroft CE, Ortí E, Bolink HJ. Shine bright or live long: substituent effects in [Cu(NĉN)(PĉP)]$^{+}$-based light-emitting electrochemical cells where NĉN is a 6-substituted 2,2′-bipyridine. J Mater Chem C 2016;4:3857–71. https://doi.org/10.1039/C5TC03725E.
[40] Leoni E, Mohanraj J, Holler M, Mohankumar M, Nierengarten I, Monti F, Sournia-Saquet A, Delavaux-Nicot B, Nierengarten JF, Armaroli N. Heteroleptic copper(I) complexes prepared from phenanthroline and bis-phosphine ligands: rationalization of the photophysical and electrochemical properties. Inorg Chem 2018;57:15537–49. https://doi.org/10.1021/acs.inorgchem.8b02879.
[41] Liu Y, You S-C, Ho C-L, Wong W-Y. Recent advances in copper complexes for electrical/light energy conversion. Coord Chem Rev 2018;375:514–57. https://doi.org/10.1016/j.ccr.2018.05.010.
[42] Doettinger F, Yang Y, Schmid M-A, Frey W, Karnahl M, Tschierlei S. Cross-coupled phenyl- and alkynyl-based phenanthrolines and their effect on the photophysical and electrochemical properties of heteroleptic Cu(I) photosensitizers. Inorg Chem 2021;60:5391–401. https://doi.org/10.1021/acs.inorgchem.1c00416.
[43] Sandoval-Pauker C, Santander-Nelli M, Dreyse P. Thermally activated delayed fluorescence in luminescent cationic copper(i) complexes. RSC Adv 2022;12:10653–74. https://doi.org/10.1039/D1RA08082B.
[44] Si Z, Li J, Li B, Liu S, Li W. High light electroluminescence of novel Cu(I) complexes. J Lumin 2009;129:181–6. https://doi.org/10.1016/j.jlumin.2008.09.014.
[45] Chen J-L, Song P, Liao J, Wen H-R, Hong R, Chen Z-N, Chic Y. Luminescent homodinuclear copper(I) halide complexes based on the 3,5-bis{6-(2,2′-dipyridyl)}pyrazole ligand. Inorg Chem Commun 2010;13:1057–60. https://doi.org/10.1016/j.inoche.2010.06.010.
[46] Hsu C-W, Lin C-C, Chung M-W, Chi Y, Lee G-H, Chou P-T, Chang C-H, Chen P-Y. Systematic investigation of the metal-structure–photophysics relationship of emissive d^{10}-complexes of group 11 elements: the prospect of application in organic light emitting devices. J Am Chem Soc 2011;133:12085–99. https://doi.org/10.1021/ja2026568.
[47] Min J, Zhang Q, Sun W, Cheng Y, Wang L. Neutral copper(i) phosphorescent complexes from their ionic counterparts with 2-(2′-quinolyl)benzimidazole and phosphine mixed ligands. Dalton Trans 2011;40:686–93. https://doi.org/10.1039/C0DT01031F.
[48] Femoni C, Muzzioli S, Palazzi A, Stagni S, Zacchini S, Monti F, Accorsi G, Bolognesi M, Armaroli N, Massi M, Valenti G, Marcaccio M. New tetrazole-based Cu(I) homo- and heteroleptic complexes with various PĉP ligands: synthesis, characterization, redox and photophysical properties. Dalton Trans 2013;42:997–1010. https://doi.org/10.1039/C2DT32056H.
[49] Bergmann L, Friedrichs J, Mydlak M, Baumann T, Nieger M, Bräse S. Outstanding luminescence from neutral copper(I) complexes with pyridyl-tetrazolate and phosphine ligands. Chem Commun 2013;49:6501–3. https://doi.org/10.1039/C3CC42280A.
[50] Zhang Q, Chen X-L, Chen J, Wu X-Y, Yu R, Lu C-Z. Photo- and electro-luminescence of four cuprous complexes with sterically demanding and hole transmitting diimine ligands. Dalton Trans 2015;44:10022–9. https://doi.org/10.1039/C5DT01108F.
[51] Chen JL, Guo ZH, Yu HG, He LH, Liu SJ, Wen HR, Wang JY. Luminescent dinuclear copper(I) complexes bearing 1,4-bis(diphenylphosphino)butane and functionalized 3-(2′-pyridyl)pyrazole mixed ligands. Dalton Trans 2016;45:696–705. https://doi.org/10.1039/C5DT03451E.
[52] Back O, Leppin J, Förster C, Heinze K. Photochemistry and redox chemistry of an unsymmetrical bimetallic copper(I) complex. Inorg Chem 2016;55:9653–62. https://doi.org/10.1021/acs.inorgchem.6b01400.
[53] Sun Y, Lemaur V, Beltrán JI, Cornil J, Huang J, Zhu J, Wang Y, Fröhlich R, Wang H, Jiang L, Zou G. Neutral mononuclear copper(I) complexes: synthesis, crystal structures, and photophysical properties. Inorg Chem 2016;55:5845–52. https://doi.org/10.1021/acs.inorgchem.6b00101.
[54] Li G, Nobuyasu RS, Zhang B, Geng Y, Yao B, Xie Z, Zhu D, Shan G, Che W, Yan L, Su Z, Dias FB, Bryce MR. Thermally activated delayed fluorescence in Cu^{I} complexes originating from restricted molecular vibrations. Chem Eur J 2017;23:11761–6. https://doi.org/10.1002/chem.201701862.
[55] Hupp B, Schiller C, Lenczyk C, Stanoppi M, Edkins K, Lorbach A, Steffen A. vSynthesis, structures, and photophysical properties of a series of rare near-IR emitting copper(I) complexes. Inorg Chem 2017;56:8996–9008. https://doi.org/10.1021/acs.inorgchem.7b00958.
[56] Bergmann L, Braun C, Nieger M, Bräse S. The coordination- and photochemistry of copper(i) complexes: variation of NĉN ligands from imidazole to tetrazole. Dalton Trans 2018;47:608–21. https://doi.org/10.1039/C7DT03682E.
[57] Bizzarri C, Arndt AP, Kohaut S, Fink K, Nieger M. Mononuclear and dinuclear heteroleptic Cu(I) complexes based on pyridyl-triazole and DPEPhos with long-lived excited-state lifetimes. J Organomet Chem 2018;871:140–9. https://doi.org/10.1016/j.jorganchem.2018.07.013.
[58] Wu Y, Han X, Qu Y, Zhao K, Wang C, Huang G, Wu H. Two Cu(I) complexes constructed by different N-heterocyclic benzoxazole ligands: syntheses, structures and fluorescent properties. J Mol Struct 2019;1191:95–100. https://doi.org/10.1016/j.molstruc.2019.04.108.
[59] Bortoluzzi M, Castro J, Girotto M, Enrichi F, Vomiero A. Luminescent copper(I) coordination polymer with 1-methyl-1*H*-benzotriazole, iodide and acetonitrile as ligands. Inorg Chem Commun 2019;102:141–6. https://doi.org/10.1016/j.inoche.2019.02.016.
[60] Ferraro V, Bortoluzzi M, Castro J, Vomiero A, You S. Luminescent Cu(I) complex with bis(indazol-1-yl)phenylmethane as chelating ligand. Inorg Chem Commun 2020;116:107894. https://doi.org/10.1016/j.inoche.2020.107894.
[61] Lüdtke N, Föller J, Marian CM. Understanding the luminescence properties of Cu (I) complexes: a quantum chemical perusal. Phys Chem Chem Phys 2020;22:23530–44. https://doi.org/10.1039/d0cp04654j.
[62] Alconchel A, Crespo O, García-Orduña P, Gimeno MC. *Closo*- or *nido*-carborane diphosphane as responsible for strong thermochromism or time activated delayed fluorescence (TADF) in [Cu(NĉN)(PĉP)]$^{0/+}$. Inorg Chem 2021;60:18521–8. https://doi.org/10.1021/acs.inorgchem.1c03092.
[63] Baranova KF, Titov AA, Smol'yakov AF, Chernyadyev AY, Filippov OA, Shubina ES. Mononuclear copper(I) 3-(2-pyridyl)pyrazole complexes: the crucial role of phosphine on photoluminescence. Molecules 2021;26:6869. https://doi.org/10.3390/molecules26226869.
[64] Grupe M, Boden P, Di Martino-Fumo P, Gui X, Bruschi C, Israil R, Schmitt M, Nieger M, Gerhards M, Klopper W, Riehn C, Bizzarri C, Diller R. Time-resolved spectroscopy and electronic structure of mono- and dinuclear pyridyl-triazole/DPEPhos-based Cu(I) complexes. Chem Eur J 2021;27:15252–71. https://doi.org/10.1002/chem.202102760.
[65] Pathaw L, Maheshwaran D, Nagendraraj T, Khamrang T, Velusamy M, Mayilmurugan R. Tetrahedral copper(I) complexes of novel N,N-bidentate ligands and photophysical properties. Inorg Chim Acta 2021;514:119999. https://doi.org/10.1016/j.ica.2020.119999.
[66] Ferraro V, Castro J, Agostinis L, Bortoluzzi M. Luminescent heteroleptic copper(I) complexes with polydentate benzotriazolyl-based ligands. Transit Met Chem 2021;46:391–402. https://doi.org/10.1007/s11243-021-00458-4.
[67] Castro J, Ferraro V, Bortoluzzi M. Visible-emitting Cu(i) complexes with N-functionalized benzotriazole-based ligands. New J Chem 2022;46:18938–51. https://doi.org/10.1039/D2NJ03165E.
[68] Chai W, Hong M, Song L, Jia G, Shi H, Guo J, Shu K, Guo B, Zhang Y, You W, Chen X. Three reversible polymorphic copper(I) complexes triggered by ligand conformation: insights into polymorphic crystal habit and luminescent properties. Inorg Chem 2015;54:4200–7. https://doi.org/10.1021/ic502709b.
[69] Tao X-D, Chai W-X, Song L, Wei Q-H, Shi H-S, Qin L-S. Two luminescent pseudo-polymorphic cuprous complexes with different optical properties: synthesis, characterization and TD-DFT calculations. Polyhedron 2018;144:36–43. https://doi.org/10.1016/j.poly.2017.12.039.
[70] Wang D-D, Song L, Wang Y-Y, Guo J-Y, Shen H-Y, Wang X-R, Chai W-X. Heteroleptic $[Cu(NN)P_2]^{+}$-type cuprous complexes and their structural modulation on phosphorescent color: synthesis, structural characterization, properties, and theoretical calculations. Appl Organomet Chem 2020;34:e5561. https://doi.org/10.1002/aoc.5561.
[71] Dai D-Q, Song L, Liang Y, Wang J-T, Zhou Y-M, Shen H-Y, Chai W-X. Heteroleptic cuprous complexes of a diimine MePBO ligand and their structure influence on phosphorescent color: syntheses, structure characterizations, properties and TD-DFT calculations. Z Anorg Allg Chem 2021;647:1896–905. https://doi.org/10.1002/zaac.202100114.
[72] Nohara I, Wegeberg C, Devereux M, Prescimone A, Housecroft CE, Constable EC. The surprising effects of sulfur: achieving long excited-state lifetimes in heteroleptic copper(I) emitters. J Mater Chem C 2022;10:3089–102. https://doi.org/10.1039/D1TC05591G.
[73] Papaefstathiou GS, Tsohos A, Raptopoulou CP, Terzis A, Psycharis V, Gatteschi D, Perlepes SP. Crystal engineering: stacking interactions control the crystal structures of benzothiadiazole (btd) and its complexes with copper(II) and copper (I) chlorides. Cryst Growth Des 2001;1:191–4. https://doi.org/10.1021/cg010284e.
[74] Munakata M, Kuroda-Sowa T, Maekawa M, Nakamura M, Akiyama S, Kitagawa S. Architecture of 2D sheets with six-membered rings of coppers interconnected by 2,1,3-benzothiadiazoles and a layered structure composed of the 2D sheets. Inorg Chem 1994;33:1284–91. https://doi.org/10.1021/ic00085a013.
[75] Fang Y, Zhu K, Teat SJ, Reid OG, Hei X, Zhu K, Fang X, Li M, Sojdak CA, Cotlet M, Li J. Robust and highly conductive water-stable copper iodide-based hybrid single crystals. Chem Mater 2022;34:10040–9. https://doi.org/10.1021/acs.chemmater.2c02490.
[76] Munakata M, He H, Kuroda-Sowa T, Maekawa M, Suenaga Y. Dicopper complexes derived from 4-amino-2,1,3-benzothiadiazole with versatile co-ordination number and geometry. J Chem Soc Dalton Trans 1988:1499–502. https://doi.org/10.1039/A800549D.
[77] Sukhikh TS, Khisamov RM, Bashirov DA, Vyu Komarov, Molokeev MS, Ryadun AA, Benassi E, Konchenko SN. Tuning of the coordination and emission properties of 4-amino-2,1,3-benzothiadiazole by introduction of diphenylphosphine group. Cryst Growth Des 2020;20:5796–807. https://doi.org/10.1021/acs.cgd.0c00406.
[78] Khisamov R, Sukhikh T, Bashirov D, Ryadun A, Konchenko S. Structural and photophysical properties of 2,1,3-benzothiadiazole-based phosph(III)azane and its complexes. Molecules 2020;25:2428. https://doi.org/10.3390/molecules25102428.
[79] Ferraro V, Girotto M, Bortoluzzi MN. *N*-Dimethyl-4-amino-2,1,3-benzothiadiazole: synthesis and luminescent solvatochromism. Chem Process 2022;8:87. https://doi.org/10.3390/ecsoc-25-11658.
[80] Armarego WLF, Perrin DD. Purification of laboratory chemicals. Oxford: Butterworth-Heinemann; 1996.
[81] Ferraro V, Castro J, Trave E, Bortoluzzi M. Preparation, reactivity and photoluminescence of copper(I) borohydride complexes with bis[(2-diphenylphosphino)phenyl] ether as chelating ligand. J Organomet Chem 2022;957:122171. https://doi.org/10.1016/j.jorganchem.2021.122171.

[82] Bianchini C, Ghilardi CA, Meli A, Midollini S, Orlandini A. Reactivity of copper(I) tetrahydroborates toward carbon dioxide and carbonyl sulfide. Structure of (triphos)Cu(.eta.1-O2CH). Inorg Chem 1985;24:924–31. https://doi.org/10.1021/ic00200a025.

[83] Kubas GJ, Monzyk B, Crumblis AL. Tetrakis(Acetonitrile)Copper(1+) hexafluorophosphate(1-). Inorg Synth 1990;28:68–70. https://doi.org/10.1002/9780470132593.ch15.

[84] Keller RN, Wycoff HD, Marchi LE. Copper(I) chloride. Inorg Synth 1946;2:1–4. https://doi.org/10.1002/9780470132333.ch1.

[85] Bruker. APEX3, smart, SAINT. Madison, Wisconsin, USA: Bruker AXS Inc.; 2015.

[86] McArdle P. *Oscail*, a program package for small-molecule single-crystal crystallography with crystal morphology prediction and molecular modelling. J Appl Crystallogr 2017;50:320–6. https://doi.org/10.1107/S1600576716018446.

[87] Sheldrick GM. *Shelxt* - integrated space-group and crystal-structure determination. Acta Crystallogr 2015;A71:3–8. https://doi.org/10.1107/S2053273314026370.

[88] Sheldrick GM. Crystal structure refinement with *SHELXL*. Acta Crystallogr 2015;C71:3–8. https://doi.org/10.1107/S2053229614024218.

[89] Spek AL. *checkCIF* validation ALERTS: what they mean and how to respond. Acta Crystallogr 2020;E76:1–11. https://doi.org/10.1107/S2056989019016244.

[90] Yu HS, He X, Li SL, Truhlar DG. MN15: a Kohn–Sham global-hybrid exchange–correlation density functional with broad accuracy for multi-reference and single-reference systems and noncovalent interactions. Chem Sci 2016;7:5032–51. https://doi.org/10.1039/C6SC00705H.

[91] Weigend F, Ahlrichs R. Balanced basis sets of split valence, triple zeta valence and quadruple zeta valence quality for H to Rn: design and assessment of accuracy. Phys Chem Chem Phys 2005;7:3297–305. https://doi.org/10.1039/B508541A.

[92] Cossi M, Rega N, Scalmani G, Barone V. Energies, structures, and electronic properties of molecules in solution with the C-PCM solvation model. J Comput Chem 2003;24:669–81. https://doi.org/10.1002/jcc.10189.

[93] Barone V, Cossi M. Quantum calculation of molecular energies and energy gradients in solution by a conductor solvent model. J Phys Chem A 1998;102:1995–2001. https://doi.org/10.1021/jp9716997.

[94] Ullrich CA. Time-dependent density functional theory. Oxford: Oxford University Press; 2012.

[95] Frisch MJ, Trucks GW, Schlegel HB, Scuseria GE, Robb MA, Cheeseman JR, Scalmani G, Barone V, Petersson GA, Nakatsuji H, Li X, Caricato M, Marenich AV, Bloino J, Janesko BG, Gomperts R, Mennucci B, Hratchian HP, Ortiz JV, Izmaylov AF, Sonnenberg JL, Williams-Young D, Ding F, Lipparini F, Egidi F, Goings J, Peng B, Petrone A, Henderson T, Ranasinghe D, Zakrzewski VG, Gao J, Rega N, Zheng G, Liang W, Hada M, Ehara M, Toyota K, Fukuda R, Hasegawa J, Ishida M, Nakajima T, Honda Y, Kitao O, Nakai H, Vreven T, Throssell K, Montgomery Jr JA, Peralta JE, Ogliaro F, Bearpark MJ, Heyd JJ, Brothers EN, Kudin KN, Staroverov VN, Keith TA, Kobayashi R, Normand J, Raghavachari K, Rendell AP, Burant JC, Iyengar SS, Tomasi J, Cossi M, Millam JM, Klene M, Adamo C, Cammi R, Ochterski JW, Martin RL, Morokuma K, Farkas O, Foresman JB, Fox DJ. Gaussian 16, revision C.01. Wallingford CT: Gaussian, Inc.; 2016.

[96] Lu T, Chen F. Multiwfn: a multifunctional wavefunction analyzer. J Comput Chem 2012;33:580–92. https://doi.org/10.1002/jcc.22885.

[97] Liu Z, Lu T, Chen Q. An sp-hybridized all-carboatomic ring, cyclo[18]carbon: electronic structure, electronic spectrum, and optical nonlinearity. Carbon 2020;165:461–7. https://doi.org/10.1016/j.carbon.2020.05.023.

[98] Falivene L, Cao Z, Petta A, Serra L, Poater A, Oliva R, Scarano V, Cavallo L. Towards the online computer-aided design of catalytic pockets. Nat Chem 2019;11:872–9. https://doi.org/10.1038/s41557-019-0319-5.

[99] Cordero B, Gómez V, Platero-Prats AE, Revés M, Echeverría J, Cremades E, Barragán F, Alvarez S. Covalent radii revisited. Dalton Trans 2008:2832–8. https://doi.org/10.1039/b801115j.

[100] Legon AC, Walker NR. What's in a name? 'Coinage-metal' non-covalent bonds and their definition. Chem Phys Phys Chem 2018;20:19332–8. https://doi.org/10.1039/c8cp03432j.

[101] Rahm M, Hoffmann R, Ashcroft NW. Atomic and ionic radii of elements 1–96. Chem Eur J 2016;22:14625–32. https://doi.org/10.1002/chem.201602949.

[102] Dai Y, Zhang Y, Tian J, Liu Z. Aquabis-(triphenyl-phosphine-*kP*)copper(I) tetrafluoridoborate. Acta Crystallogr 2009;E65:m1001. https://doi.org/10.1107/S1600536809029559.

[103] Titov AA, Filippov OA, Smol'yakov AF, Averin AA, Shubina ES. Copper(I) complex with BINAP and 3,5-dimethylpyrazole: synthesis and photoluminescent properties. Mendeleev Commun 2019;29:570–2. https://doi.org/10.1016/j.mencom.2019.09.031.

[104] Bachechi F, Burini A, Fontani M, Galassi R, Macchioni A, Pietroni BR, Zanello P, Zuccaccia C. Solid state and solution investigations of derivatives of Group 11 metal ions with 1-benzyl-2-imidazolyldiphenylphosphine (L). Electrochemical behavior of $[M_2L_3]^{2+}$ ($M=Cu^{I}$; Ag^{I}) and $[AuL_2]^{+}$ complexes. Inorg Chim Acta 2001;323:45–54. https://doi.org/10.1016/S0020-1693(01)00582-5.

[105] Royzman DE, Noviello AM, Henline KM, Pike RD, Killarney JP, Patterson HH, Crawford C, Assefa Z. Structure, luminescence, and vapochromism of bridged cationic copper(I) dimers and polymers. J Inorg Organomet Polym 2014;24:66–77. https://doi.org/10.1007/s10904-013-9978-7.

[106] Jin Q-H, Chen L-M, Li P-Z, Deng S-F, Wang R. The synthesis, structure, and characterization of three novel 1D nitrogen-heterocyclic copper(I)-diphosphine polymers. Inorg Chim Acta 2009;362:5224–30. https://doi.org/10.1016/j.ica.2009.09.035.

[107] Shamsieva AV, Musina EI, Gerasimova TP, Strelnik ID, Strelnik AG, Kolesnikov IE, Kalinichev AA, Islamov DR, Samigullina AI, Lönnecke P, Katsyuba SA, Hey-Hawkins E, Karasik AA, Sinyashin OG. Triple-bridged helical binuclear copper(i) complexes: head-to-head and head-to-tail isomerism and the solid-state luminescence. Dalton Trans 2020;49:11997–2008. https://doi.org/10.1039/D0DT01843K.

[108] McCormick T, Jia WL, Wang S. Phosphorescent Cu(I) complexes of 2-(2'-pyridylbenzimidazolyl)benzene: impact of phosphine ancillary ligands on electronic and photophysical properties of the Cu(I) complexes. Inorg Chem 2006;45:147–55. https://doi.org/10.1021/ic051412h.

[109] Chen J-L, Zeng X-H, Luo Y-S, Wang W-M, He L-H, Liu S-J, Wen H-R, Huang S, Liu L, Wong WY. Synthesis, structure, and photophysics of copper(I) triphenylphosphine complexes with functionalized 3-(2′-pyrimidinyl)-1,2,4-triazole ligands. Dalton Trans 2017;46:13077–87. https://doi.org/10.1039/C7DT02848B.

[110] Mao S, Han X, Li C, Xu Y, Shen K, Shi X, Wu H. Cu(I) complexes regulated by N-heterocyclic ligands: syntheses, structures, fluorescence and electrochemical properties. Spectrochim Acta, Part A 2018;203:408–14. https://doi.org/10.1016/j.saa.2018.06.003.

[111] Bera JK, Nethaji M, Samuelson AG. Synthesis and structures of oxyanion encapsulated copper(I)−dppm complexes (dppm = bis(diphenylphosphino) methane). Inorg Chem 1999;38:1725–35. https://doi.org/10.1021/ic9801589.

[112] Li D, Li R-Z, Ni Z, Qi Z-Y, Feng X-L, Cai J-W. Synthesis and crystal structure of photoluminescent copper(I)–phosphine complexes with oxygen and nitrogen donor ligands. Inorg Chem Commun 2003;6:469–73. https://doi.org/10.1016/S1387-7003(03)00015-7.

[113] Lotito KJ, Peters JC. Efficient luminescence from easily prepared three-coordinate copper(i) arylamidophosphines. Chem Commun 2010;46:3690–2. https://doi.org/10.1039/c000818d.

[114] Annan TA, Kickham JE, Tuck DG. The direct electrochemical synthesis of the novel copper(I) complex $Cu_2[OC_6Cl_4(OH)]_2[(C_6H_5)_2PCH_2P(C_6H_5)_2]_2$. Can J Chem 1991;69:251–6. https://doi.org/10.1139/v91-040.

[115] Ward SC, Sadiq G. Introduction to the Cambridge Structural Database – a wealth of knowledge gained from a million structures. CrystEngComm 2020;22:7143–4. https://doi.org/10.1039/D0CE90154G.

[116] Díez J, Pilar Gamasa M, Gimeno J, Tiripicchio A, Tiripicchio Camellini M. Binuclear copper(I) complexes containing bis(diphenylphosphino)methane bridging ligands: crystal structure of $[Cu_2(\mu\text{-dppm})_2(MeCN)_4][ClO_4]_2$. J Chem Soc Dalton Trans 1987:1275–8. https://doi.org/10.1039/DT9870001275.

[117] Liu H, Calhorda MJ, Drew MGB, Félix V, Novosad J, Veiros LF, Fabrizi de Biani F, Zanello P. New Cu(I) and Ag(I) binuclear complexes containing the dppa ligand. J Chem Soc Dalton Trans 2002:4365–74. https://doi.org/10.1039/B205922N.

[118] Moussa ME, Evariste S, Krämer B, Réau R, Scheer M, Lescop C. Can coordination-driven supramolecular self-assembly reactions Be conducted from fully aliphatic linkers? Angew Chem Int Ed 2018;57:795–9. https://doi.org/10.1002/anie.201709119.

[119] Bianchi R, Gervasio G, Marabello D. Experimental electron density analysis of $Mn_2(CO)_{10}$: metal−Metal and Metal−Ligand bond characterization. Inorg Chem 2000;39:2360–6. https://doi.org/10.1021/ic991316e.

[120] Lepetit C, Fau P, Fajerwerg K, Kahn ML, Silvi B. Topological analysis of the metal-metal bond: a tutorial review. Coord Chem Rev 2017;345:150–62. https://doi.org/10.1016/j.ccr.2017.04.009.

[121] Yang X, Chin RM, Hall MB. Protonating metal-metal bonds: changing the metal-metal interaction from bonding, to nonbonding, and to antibonding. Polyhedron 2022;212:115585. https://doi.org/10.1016/j.poly.2021.115585.

[122] Yam VW-W, Au VK-M, Leung SY-L. Light-emitting self-assembled materials based on d^8 and d^{10} transition metal complexes. Chem Rev 2015;115:7589–728. https://doi.org/10.1021/acs.chemrev.5b00074.

[123] Hupp B, Nitsch J, Schmitt T, Bertermann R, Edkins K, Hirsch F, Fischer I, Auth M, Sperlich A, Steffen A. Stimulus-triggered formation of an anion–cation exciplex in copper(I) complexes as a mechanism for mechanochromic phosphorescence. Angew Chem Int Ed 2018;57:13671–5. https://doi.org/10.1002/anie.201807768.

[124] Liske A, Wallbaum L, Hölzel T, Föller J, Gernert M, Hupp B, Ganter C, Marian CM, Steffen A. Cu–F interactions between cationic linear N-heterocyclic carbene copper(I) pyridine complexes and their counterions greatly enhance blue luminescence efficiency. Inorg Chem 2019;58:5433–45. https://doi.org/10.1021/acs.inorgchem.9b00337.

[125] Xing G, Du T, Liu S, Ma Y, Zhao Q. Controlling the photophysical properties of ionic transition-metal complexes through various counterions. Chem Commun 2022;58:12286–96. https://doi.org/10.1039/D2CC04651B.

[126] Meyer M, Mardegan L, Tordera D, Prescimone A, Sessolo M, Bolink HJ, Constable EC, Housecroft CE. A counterion study of a series of [Cu(PĉP)(NĉN)][A] compounds with bis(phosphane) and 6-methyl and 6,6′-dimethyl-substituted 2,2′-bipyridine ligands for light-emitting electrochemical cells. Dalton Trans 2021;50:17920–34. https://doi.org/10.1039/D1DT03239A.

[127] Nolden O, Kremper J, Haselbach W, Morshedi M, Guhl J, Schmeinck P, Marian CM, Ganter C, Gilch P. Femtosecond spectroscopy and quantum chemistry of a linearly coordinated copper(I) carbene complex. ChemPhotoChem 2022:e202200231. https://doi.org/10.1002/cptc.202200231.

[128] Liske A, Wallbaum L, Hölzel T, Föller J, Gernert M, Hupp B, Ganter C, Marian CM, Steffen A. Cu−F interactions between cationic linear N-heterocyclic carbene copper(I) pyridine complexes and their counterions greatly enhance blue luminescence efficiency. Inorg Chem 2019;58:5433–55. https://doi.org/10.1021/acs.inorgchem.9b00337.

[129] Englman R, Jortner J. The energy gap law for radiationless transitions in large molecules. Mol Phys 1970;18:145–64. https://doi.org/10.1080/00268977000100171.
[130] Kober EM, Caspar JV, Lumpkin RS, Meyer TJ. Application of the energy gap law to excited-state decay of osmium(II)-polypyridine complexes: calculation of relative nonradiative decay rates from emission spectral profiles. J Phys Chem 1986;90:3722–34. https://doi.org/10.1021/j100407a046.
[131] Schubert EF. Light-emitting diodes. second ed. Cambridge: Cambridge University Press; 2006. p. 292–303.
[132] Scrivanti A, Bortoluzzi M, Morandini A, Dolmella A, Enrichi F, Mazzaro R, Vomiero A. Luminescent europium(III) complexes containing an electron rich 1,2,3-triazolyl-pyridyl ligand. New J Chem 2018;42:11064–72. https://doi.org/10.1039/c8nj01390j.
[133] Bortoluzzi M, Gobbo A. 1,3-Dimethyl-2-phenyl-1,3-diazaphospholidine-2-oxide as ligand for the preparation of luminescent lanthanide complexes. J Coord Chem 2019;72:1524–36. https://doi.org/10.1080/00958972.2019.1608440.
[134] Bortoluzzi M, Gobbo A, Palù A, Enrichi F, Vomiero A. Luminescent lanthanide complexes with phosphoramide and arylphosphonic diamide ligands. Chem Pap 2020;74:3693–704. https://doi.org/10.1007/s11696-019-00799-6.
[135] Bortoluzzi M, Ferraro V, Sartor F. Photoluminescence of homoleptic lanthanide complexes with tris(benzotriazol-1-yl)borate. J Fluoresc 2021;31:1433–43. https://doi.org/10.1007/s10895-021-02772-7.
[136] Bortoluzzi M, Di Vera A, Pietrobon L, Castro J. Seven- and eight-coordinate lanthanide(III) amidophosphate complexes: synthesis, characterization and photoluminescence. J Coord Chem 2021;74:1466–81. https://doi.org/10.1080/00958972.2021.1916001.
[137] Li C, Mackenzie CFR, Said SA, Pal AK, Haghighatbin MA, Babaei A, Sessolo M, Cordes DB, Slawin AMZ, Kamer PCJ, Bolink HJ, Hogan CF, Zysman-Colman E. Wide-bite-angle diphosphine ligands in thermally activated delayed fluorescent copper(I) complexes: impact on the performance of electroluminescence applications. Inorg Chem 2021;60:10323–39. https://doi.org/10.1021/acs.inorgchem.1c00804.
[138] Smith CS, Mann KR. Exceptionally long-lived luminescence from [Cu(I)(isocyanide)$_2$(phen)]$^+$ complexes in nanoporous crystals enables remarkable oxygen gas sensing. J Am Chem Soc 2012;134:8786–9. https://doi.org/10.1021/ja302807s.
[139] Małecki JG, Łakomska I, Maroń A, Szala M, Fandzloch M, Nycz JE. Phosphorescent emissions of phosphine copper(I) complexes bearing 8-hydroxyquinoline carboxylic acid analogue ligands. J Lumin 2015;161:382–8. https://doi.org/10.1016/j.jlumin.2015.01.041.
[140] Yersin H, Rausch AF, Czerwieniec R, Hofbeck T, Fischer T. The triplet state of organo-transition metal compounds. Triplet harvesting and singlet harvesting for efficient OLEDs. Coord Chem Rev 2011;255:2622–52. https://doi.org/10.1016/j.ccr.2011.01.042.
[141] Alkan-Zambada M, Constable EC, Housecroft CE. The role of percent volume buried in the characterization of copper(I) complexes for lighting purposes. Molecules 2020;25:2647. https://doi.org/10.3390/molecules25112647.